# *Superhydrophobic Fatty Acid-Based Spray Coatings with Dual-mode Antifungal Activity*

*Elena Prudnikov* [a], *Hanan Abu Hamad* [b], *Iryna Polishchuk* [a], *Alexander Katsman* [a], *Ester Segal* [b*] *and Boaz Pokroy* [a*]

[a*] Department of Materials Science and Engineering, Technion − Israel Institute of Technology, 3200003 Haifa, Israel. E-mail: bpokroy@technion.ac.il; Tel: +972-4-829-4584

[b] Faculty of Biotechnology and Food Engineering, Technion − Israel Institute of Technology, 3200003 Haifa, Israel

**KEYWORDS:** superhydrophobic, self-cleaning, coatings, fatty acids, spray coating, active components incorporation and release, antimicrobial, antifungal

**Abstract**

Superhydrophobicity, a natural phenomenon commonly observed in plants and insects, imparts diverse functionalities, including self-cleaning capabilities. Nature's design of a superhydrophobic surface relies on a combination of surface chemistry and hierarchical roughness at micro- and nano-scales. The growing interest in artificial superhydrophobic surfaces is driven by their unique properties and additional functionalities, such as anti-icing, corrosion prevention, and anti-biofouling properties. While many studies show the antibacterial properties of superhydrophobic surfaces, only a handful focus on fungi. However, fungal infections are becoming increasingly prevalent, driven by global warming and the growing resistance of fungi to conventional fungicides. Notably, among novel superhydrophobic surfaces, those made with natural, non-toxic, and environmentally friendly compounds via facile manufacturing methods, offer significant advantages and align with sustainable engineering practices.

In this study, we developed an easy-to-apply, sprayable bi-modal coatings. These superhydrophobic antifungal coatings, made of long-chain fatty acid, can be combined with medium-chain fatty acids to enhance the antifungal activity against the model phytopathogen *Botrytis cinerea*. We investigate the effect of incorporating sorbic and caprylic fatty acids in various concentrations on the structure, physical properties, stability, and applicability of stearic acid-based coatings. We show that depending on the composition, the antifungal activity of the coatings can be tuned, ranging from complete passive antibiofouling to a dominant fungicidal action against *Botrytis cinerea.*

This is made possible by the combination of the superhydrophobic coating's hierarchical structure and the incorporation of potent medium-chain fatty acids. We believe these coatings offer a sustainable solution for protecting various surfaces from fungal infections and represent a promising alternative to conventional fungicides.

## Introduction

Superhydrophobicity, commonly referred to as the "Lotus effect", is a phenomenon widely found in Nature, especially among plants and insects.[1–4] The Lotus plant has been extensively studied over the last decades for its unique wetting properties, serving as a foundation for further research on superhydrophobic natural surfaces and the development of artificial man-made analogs.[1,5–7] Organisms employ this strategy to achieve diverse functionalities, including self-cleaning capabilities and improved flight performance.[6,8] Superhydrophobic surfaces, however, can exhibit additional functionalities such as thermal insulation, corrosion prevention, anti-fouling properties, anti-icing, anti-fogging, and more.[1,2,9–14] This unique behavior arises from the interplay between the two key factors: surface chemistry and surface roughness.[1–3] Hydrophobic molecules on the surface hinder the formation of strong physical bonds with water, which is essential for superhydrophobicity but insufficient on its own.[1,2,15,16] The synergy between the appropriate chemistry and a combination of micro- and nano-scale roughness facilitates the Cassie-Baxter state, in which water droplets make minimal contact with the substrate, resting primarily on a layer of air. The latter configuration results in contact angles exceeding 150°, characteristic of superhydrophobicity.[1,2,15–17] However, not all superhydrophobic surfaces serve a similar function. For instance, the Lotus plant demonstrates a self-cleaning mechanism, where droplets roll off the surface and collect dust particles along the way. In contrast, superhydrophobic rose petals show a pinning phenomenon, where water droplets remain adhered to the surface.[3,18,19] The difference in these two superhydrophobic surfaces lies in their contact angle hysteresis (CAH), defined as the difference between the advancing and the receding contact angles. The Lotus effect, characterized by a CAH of less than 10º, creates a low-adhesion surface that enables water droplets to roll off easily, thereby enhancing self-cleaning properties.[1][3] Conversely, the Rose petal effect related to a high CAH as a result of the surface roughness and strong van der Waals and capillary forces, causing droplets to remain pinned.[18,19] Therefore, low CAH is essential for achieving low adhesion and self-cleaning property on artificial superhydrophobic surfaces.

Various methods are employed to create superhydrophobic surfaces or other self-cleaning strategies including deposition techniques, lithography and templating methods, sol-gel, plasma and chemical etching, electrochemical processes, 3D printing, SLIPS, and others.[20–26] Our group has developed a bio-inspired method to form crystalline superhydrophobic surfaces by self-assembling paraffin waxes deposited through a thermal deposition, mimicking the wax crystals covering the lotus leaves.[27,28] The properties of these surfaces can be accurately tuned, and demonstrate excellent anti-biofouling behavior.[29–32] Building on this, we explored fatty acids as an alternative material for creating superhydrophobic surfaces through molecular self-assembly.[33] Fatty acids offer several advantages,

including low cost, natural abundance in biological systems (including the human body), and well-documented antimicrobial properties, although the exact mechanism behind these properties remains not fully understood.[34,35] Recently, fatty acids have gained significant attention as a formulation component for various superhydrophobic surfaces, including fabrics and edible coatings.[36–42] Our previous study demonstrated the feasibility of using a spray coating method to form superhydrophobic and self-cleaning surfaces with hierarchical roughness using a solvent-based formulation comprising long chain saturated fatty acids (16-20 carbons).[33] We showed that these fatty acid coatings provided protection against *E. coli* and *L. innocua* due to their unique surface morphology and roughness despite the lack of the intrinsic antibacterial properties of the powdered fatty acids.[33] Shorter fatty acids (≤10 carbons), unlike long-chain fatty acids (≥12 carbons) are known for their more potent inherent antimicrobial activity.[34,35] Likewise, unsaturation of the fatty acid chain increases the antimicrobial potency when the same chain length is considered.[34,35] However, the physical properties of fatty acids, determined by their molecular length and degree of saturation, significantly impact their suitability for forming superhydrophobic coatings.[34,35,43] Shorter-chain fatty acids tend to be more hydrophilic and often exist in liquid form, rendering them unsuitable as standalone components for superhydrophobic coatings.

In this study, we expand the previously introduced concept of superhydrophobic fatty acid coatings by developing coatings that incorporate multiple fatty acids for enhanced antimicrobial activity using a facile spray-coating method. Two medium-chain fatty acids (MCFAs), sorbic and caprylic acids, were selected as potent additives to the long-chain stearic acid-based coating. Sorbic acid ($C_6H_8O_2$) is a solid polyunsaturated fatty acid well known for its antimicrobial properties and is widely used as a food preservative.[44,45] Caprylic acid ($C_8H_{16}O_2$), a liquid saturated fatty acid, which is an effective antimicrobial agent against both bacteria and fungi.[46–48] This study not only examines the structure, morphology, and crystallography of these bi-modal surfaces and the impact of medium-chain fatty acids on the performance of long-chain fatty acid coatings, but also explores the antifungal properties of both single-component and newly developed multi-component fatty acid coatings.

With global warming, the detrimental impact of fungi on humans is on the rise[49], inducing emergence of new fungal pathogens, spread, and antifungal resistance.[50] Fungi directly threaten human health, as causing severe invasive infections that are estimated to result in over 2.5 million deaths globally.[51] They also account for indirect economic effects.[52] Yet, despite these staggering figures, there are only a handful of reports which explore the use of bioinspired patterned surfaces to mitigate fungal pathogens on various surfaces.[53]

In this study, *Botrytis cinerea* (*B. cinerea*), commonly known as gray mold, was selected as a model fungus. *B. cinerea* is a prevalent necrotrophic fungus that attacks plants through various mechanisms, making it difficult to control.[54,55] Mitigating fungal infections, including those caused by *Botrytis cinerea*, is particularly challenging due to their ability to develop resistance to commonly used fungicides.[55] Additionally, conventional fungicides often pose risks to both human health and environment, which leads to regulatory restrictions.[55] Therefore, there is an urgent need for effective and sustainable disease management strategies to reduce the reliance on synthetic fungicides.[55–57] Fatty acids emerge as promising antifungal agents as they are less likely to induce resistance development and are environmentally friendly.[47,48]

Herein, we correlate the compositional, structural, and wetting properties of our developed single- and multi-component fatty acid superhydrophobic coatings with their effectiveness against *Botrytis cinerea*, demonstrating their ability to resist fungal infections.

## Experimental

### ***Materials***

Stearic acid (97%, Merck, Germany), sorbic acid (99%, Thermo Scientific, USA), and caprylic acid (99%, Acros Organics, USA) were used for the coating formation. Diethyl ether (stab. BHT, Bio-Lab, Israel) was used as a solvent.

### ***Coating formation***

A stearic acid solution at 20 mg/mL concentration was prepared by adding stearic acid to diethyl ether, and stirring was performed until complete dissolution was achieved. Then, the required amount of sorbic acid or caprylic acid, according to the desired coating composition, was added to the stearic acid solution and manually mixed to achieve complete dissolution (see details in SI 1). The solutions were applied onto microscope glass slides using a commercially available spray gun (Airbrush BRIXO Tank Top Airforce, 600 cc, nozzle size 1.4 µm) connected to compressed air at a pressure of 6 bar. A constant volume of 50 mL was sprayed onto a standard glass slide (7.5 × 2.5 $cm^2$) to fabricate the coatings. Samples were characterized and stored in a separate petri dish at ambient conditions.

### ***Characterization***

Electron microscopy:

The coating`s morphology was studied using a high-resolution scanning electron microscope (HR-SEM)—Zeiss Ultra Plus FEG-SEM. 1 KV voltage was applied during the imaging. Prior to the measurement, the samples were coated using a carbon coater.

Surface roughness:

Surface roughness measurements and surface visualization were performed using a dynamic confocal microscope (Leica DCM3D or Sensofar Sneox). The confocal microscope data was processed using SensoMap Turbo 5.1.1.5450 or SensoView 2.2.2 software, respectively, to obtain surface visualizations and roughness parameters.

Wetting properties:

The wetting properties, contact angle, and contact angle hysteresis were measured using Attension Theta Lite tensiometer and high-purity water. A volume of 7 µL was used for static contact angle measurements.

Structural analysis:

Structural characterization of the coatings was performed by X-ray diffraction (XRD) using a Rigaku SmartLab 9kW diffractometer in a parallel beam theta-2theta measurement mode. High-resolution powder X-ray diffraction (HR-PXRD) was performed on beamline ID22 of the European Synchrotron Radiation Facility (ESRF) in Grenoble, France. The coatings were detached from a substrate (mechanically scraped off) to perform these measurements, and the resulting powder was measured inside a spinning capillary.

***Coatings on a Flexible Porous Substrate (Cellulose Filter Paper):***

The coating on the filter papers was prepared following the previously described procedure, with 100 mL of the solution sprayed over a standard 90 mm petri dish containing seven filter papers fixed in place (Whatman, grade 1, 25 mm, China). The properties of the coatings deposited on the paper substrates were characterized as described above.

To assess their long-term superhydrophobic performance, a 7 µL water droplet, colored with methyl orange for easier observation, was placed on the coated filter papers. The samples were then covered with a petri dish to minimize water evaporation during observation.

To study the performance of the coatings under a challenging water exposure, the coated filter papers were placed, coating-side up, on the water surface, allowing the uncoated side of the filter paper to readily absorb water. A water droplet (7 µL) stained with methyl orange was placed on the coated

moist substrate and the wetting properties of the coatings were monitored over time to evaluate their durability and functionality under these conditions.

***MCFAs leaching***

To study the leaching of medium-chain fatty acids (MCFAs), specifically caprylic and sorbic acids, from the coatings, similarly sized samples were used in each experimental set (square samples of approximately 1 × 1 $cm^2$ or round samples with an 18 mm diameter). Freshly coated samples were immersed in 5 mL of double-distilled water for varying durations, ranging from 15 minutes to 24 hours. After immersion, the corresponding residual aqueous medium was collected and analyzed, while the coatings morphology and properties were characterized. In another set of experiments, samples were immersed in double-distilled water for up to 11 days, and the residual aqueous medium was analyzed in a similar manner.

Absorbance measurements:

Aliquots of 200 µL were spectrophotometrically analyzed using a microplate reader (Varioskan Flash, Thermo Fisher Scientific, USA or Multiskan GO, Thermo Fisher Scientific, USA). The measurements were performed in wavelength range of 200-400 nm.

Thermogravimetric analysis (TGA):

Thermogravimetric analysis (TGA Q5000, TA Instruments, USA) was utilized to quantify the release of caprylic acid from the coatings under accelerated conditions. The coating samples were heated to 45°C in an air atmosphere, and the weight loss was monitored continuously for 10 hours. To assess the residual content of caprylic acid in the coating, the same sample was subsequently analyzed in a dynamic high-resolution mode (resolution number: 5; sensitivity value: 1). In this experiment, the sample was heated at a rate of 5 °C $min^{-1}$ up to 350°C in nitrogen atmosphere. TGA results were analyzed by Universal Analysis 200 version 4.5A build 4.5.0.5 software.

***Antifungal studies***

Fungus strain and materials:

*Botrytis cinerea (B. cinerea)*, collected from *Vitis vinifera* (isolate B05.10), was kindly supplied by Prof. Amir Sharon (Tel Aviv University, Israel). Potato dextrose agar (PDA) was supplied by Sigma-Aldrich (Israel). FUN-1 cell stain staining was obtained from Thermo Fisher Scientific Inc. (USA). Milli-Q water (18.2 MΩ·cm) were used in all experiments.

Antifungal assays:

Antifungal studies were conducted on potato dextrose agar (PDA, Sigma-Aldrich, Israel) at 24°C. Fungal spores were harvested and dispersed in 0.9% saline and the concentration of the resulting spore suspension was adjusted to $10^4$ spores $mL^{-1}$ using a hemocytometer. 100 µL of this suspension was spread on PDA plates using glass beads. 50 mg of the studied fatty acid (either as powder or liquid) was placed at the dish center and incubated at 24°C for 7 days. In the case of caprylic acid (liquid MCFA), a round hole in the agar was created with a puncher, and a volume of 55 µL (equivalent to 50 mg) of the acid was introduced. The mycelial growth was visually observed, and the diameter of the inhibited growth area was measured using a digital caliper.

The antifungal properties of the coatings were tested using cellulose filter papers (Whatman, grade 1, 25mm, China) as a substrate. Briefly, the filter papers were sterilized using UV radiation prior to the deposition of fatty acid formulations. The coated filter papers were placed on PDA plates with their coated side facing up. Mycelial agar plugs (5-mm diameter and 5-mm thickness) containing actively growing fungi were obtained from the edge of a 7-day-old *B. cinerea* culture. These plugs were placed on top of the coated samples, and the plates were incubated at 24°C for 72 hours in dark. The samples were visually analyzed, and the visible mycelial growth area was measured using a digital caliper. Experiments were done in n=6 and statistical significance was evaluated using Student's two-tail t-test, *$p < 0.05$ is considered as statistically significant. Optical microscopy (Olympus BX51) was employed to visualize the fungal mycelium and its extent of growth onto the samples. Additionally, the viability of *B. cinerea* was investigated by FUN-1 staining to differentiate between metabolically active and inactive or dead fungal cells[58–60]. Following 72 h incubation, the samples were detached from the agar plate and transferred onto microscope slides. A 10 mM stock solution of FUN-1 was diluted to a working concentration of 10 µM in distilled water, and 30 µL of this solution was applied to the filter paper. The samples were visualized using a Confocal Laser Scanning Microscope (CLSM) LSM 880 – Upright Confocal Microscope equipped with a multiline argon laser, set to an excitation wavelength of 488 nm. Z-stack images were captured along the z-axis of the samples, with emissions detected at 521 nm for the green channel and 630 nm for the red channel, facilitating the differentiation of viable from non-viable cells based on their distinct fluorescence profiles. Note that FUN-1 is a membrane-permeable fluorescent dye which is extensively used in studies of yeast and other fungi to monitor cell viability.[61] While the dye is internalized by both living and dead cells with intact plasma membranes, resulting in a diffuse yellow-green fluorescence within the cytoplasm, only in metabolically active cells, green fluorescence is converted into orange-red cylindrical intracellular structures (CIVS) providing an indicator of cell viability.

Fungal morphology onto the samples was studied by scanning electron microscopy (Zeiss Ultra Plus FEG-SEM). The samples were fixated by incubation overnight in 2% glutaraldehyde solution, followed by washing and vacuum drying.

## Results and discussion

### ***Preparation and characterization of the coatings***

Building on our previous study on the formation of saturated fatty acid-based coatings, stearic acid was selected as a representative long-chain fatty acid for the matrix. Fatty acids with shorter carbon chains and unsaturated C-C bonds exhibit increased antimicrobial activity.[34,35] However, these fatty acids are inherently less hydrophobic and, in some cases, appear in a liquid state at RT, which makes them unsuitable as single components for superhydrophobic coatings. Two MCFAs, caprylic acid and sorbic acid, were selected as additives to the stearic acid matrix to study the formation of multi-component coatings and the resulting physical properties. Sorbic acid is poly-unsaturated fatty acid with 6 carbons and is solid at ambient conditions, while caprylic acid is a saturated fatty acid with 8 carbons and is liquid at ambient conditions. Diethyl ether was used as the solvent to prepare the solution, which was applied to various surfaces using a spray-coating deposition technique.

To examine the effect of the presence of MCFAs in the coating`s composition, stearic acid solutions containing various concentrations of sorbic or caprylic acids (from 10 to 40% of the total weight of fatty acids in the solution, see details in SI 1) were spray-deposited onto glass slides. The samples were then characterized and monitored over a two-month period while stored in separate petri dishes at ambient conditions.

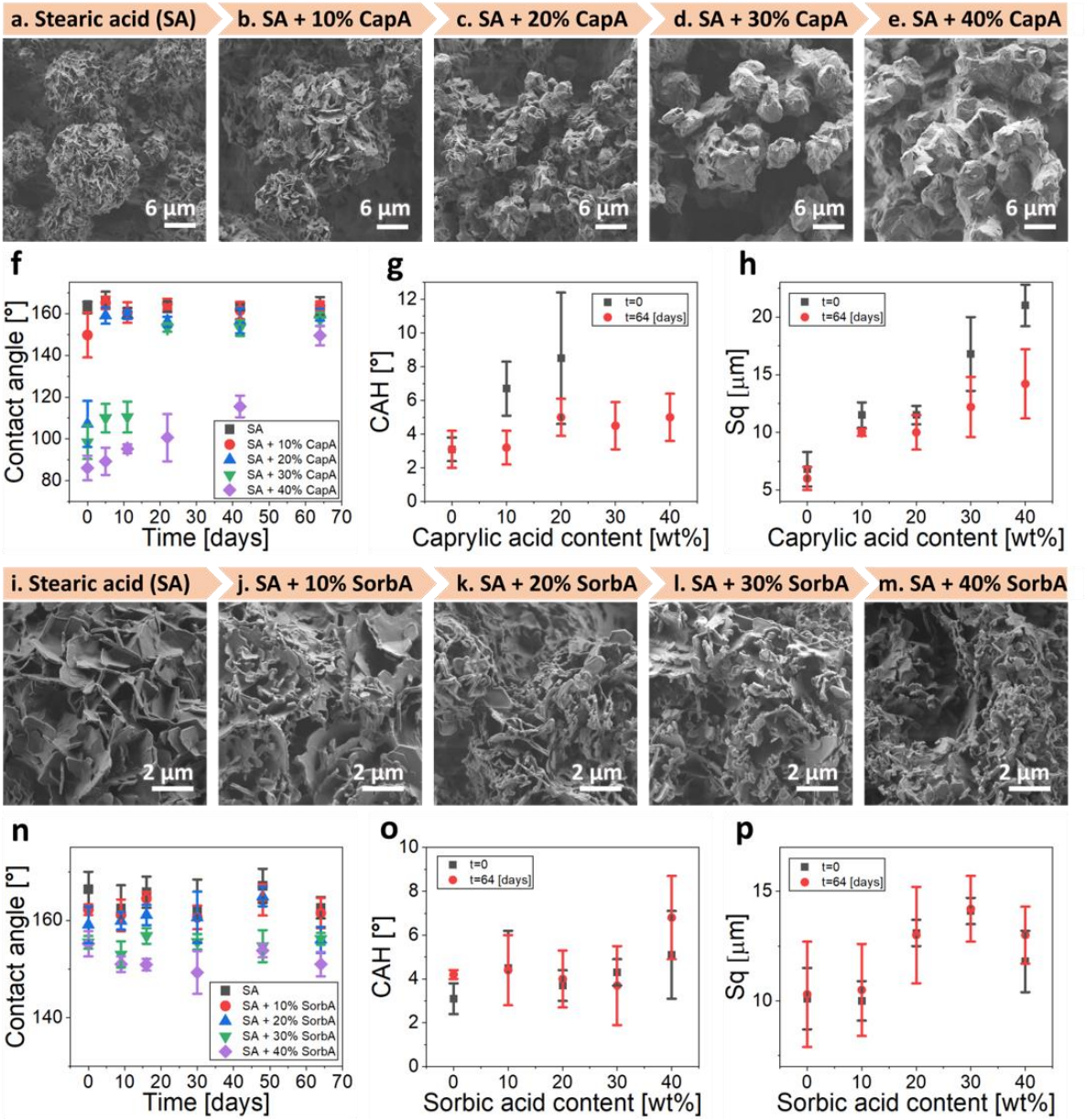


*Figure 1: (a-h) Characterization of the coatings with caprylic acid. (a-e) HR-SEM images of sprayed stearic acid coating with various amounts of caprylic acid (CapA) – 0%, 10%, 20%, 30%, and 40%, respectively. (f) Water contact angle evolution over time across different coatings. (g) Contact angle hysteresis of the different coatings at t=0 and t=64 days. (h) Roughness of the different coatings at t=0 and t=64 days. (i-p) Characterization of the coatings with sorbic acid. (i-m) HR-SEM images of sprayed stearic acid coating with various amounts of sorbic acid (SorbA) – 0%, 10%, 20%, 30%, and 40%, respectively. (n) Water contact angle evolution over time across different coatings. (o) Contact angle hysteresis of the different coatings at t=0 and t=64 days. (p) Roughness of the different coatings at t=0 and t=64 days.*

Figure 1 a-h illustrates the impact of caprylic acid addition on the final morphology and properties of the coating. The gradual increase in caprylic acid content results in the formation of smoother spheres

lacking the well-defined plate-like crystal morphology observed in pure stearic acid coating (Figure 1 a-e). The water contact angle decreases from 163° in pure stearic acid coating to 86° when the coating contains 40% caprylic acid. Additionally, CAH increases from 3° to an unmeasurable level as caprylic acid is added, resulting in the loss of superhydrophobicity and self-cleaning ability even at just 10% caprylic acid (Figure 1 f, g). The inclusion of caprylic acid with its shorter aliphatic chain and lower hydrophobicity compared to stearic acid, accounts for these changes. Moreover, these coatings demonstrate roughness values (root mean square, denoted as Sq) that progressively increase from 6.8 µm to 21.0 µm with the addition of caprylic acid. This increase indicates the presence of more pronounced crystals assembly during the spraying process, as evidenced by the corresponding HR-SEM images (Figure 1 h, a-e). Roughness parameters related to the horizontal surface dimensions,[62] namely the developed area ratio (Sdr) and the density of peaks (Spd), exhibit a similar trend, with a slight deviation observed in the 10% caprylic acid sample (see details in SI 2 a-b). This indicates the formation of a coarser and rougher surface with higher caprylic acid content, consistent with the observations from the HR-SEM images (Figure 1 a-e).

These results suggest that following the initial formation of stearic acid nuclei, the local concentration of caprylic acid around the crystals increases, probably resulting in its adsorption to the stearic acid crystals. As the solvent evaporates during spraying, the concentration of stearic acid crystals surrounded by caprylic acid in each droplet increases. It is important to note that caprylic acid is liquid at RT, giving it an oily appearance, and does not crystalize on its own. Finally, stearic acid crystals assemble via the adsorbed caprylic acid liquid layers. This process leads to stacking of the formed crystals into smooth spheres and their coalescence into clusters (Figure 1 h, a-e).

Interestingly, the CA of all coatings containing caprylic acid increases over a period of 2 months. In particular, coatings with up to 30% caprylic acid eventually demonstrate values of CA higher than 150°. The higher the caprylic acid content in the sample, the longer it takes to reach a CA of 150° (Figure 1 f). A coating with 10% caprylic acid exhibited a CA of the superhydrophobic surfaces in just 5 days, whereas 42 days were required in the case of a coating with 30% caprylic acid to showcase similar behavior. This gradual increase in CA over time, without accompanying changes in the morphology (SI 3 a-e), likely suggests the slow evaporation and release of caprylic acid from the outer surface of the coating, allowing the recovery of the superhydrophobic properties typical of pure stearic acid coating. This assumption is further evaluated and discussed (see details in Figure 4).

The addition of sorbic acid to the coating's composition had a limited effect on the on its properties. The spraying process activates solvent evaporation followed by the crystallization of both sorbic acid and stearic acid, which are crystalline solids at RT. The coating morphology is slightly altered by the

addition of sorbic acid (Figure 1 i-m). The inclusion of sorbic acid in the formulation results in the formation of smoother, less-defined crystals, which are distributed between the primary plate-like crystals that form the spherical crystal assemblies (Figure 1 i vs. j-m and lower magnification images with a larger field of view are depicted in SI 4). The effect becomes more pronounced as the amount of sorbic acid increases. Interestingly, the contact angle of the resulting coating only slightly decreases with the higher sorbic acid content, despite its relatively high solubility in water. Moreover, the contact angle remains constant over time (Figure 1 n). In contrast to the coatings with caprylic acid, all the tested compositions with sorbic acid (up to 40% w/w) showed water contact angles higher than $150^{o}$ and CAH lower than $6^{o}$ at t=0, indicating the formation of superhydrophobic surfaces demonstrating self-cleaning properties (Figure 1 n, o). Only minor deviations from the initial values, within the margin of error, were observed over time. The coating's roughness (Sq) and horizontal surface parameters (Sdr and Spd) are less impacted by the presence of sorbic acid compared to coatings containing caprylic acid. (Figure 1 h, p, SI 2 d-e). No significant changes in the morphology of the various samples were observed after 2 months of storage (SI 3 f-j).

To determine whether the presence of caprylic or sorbic acids alters the coating's structure, we conducted X-ray diffraction in θ-2θ mode, using a wavelength of 1.54 Å.

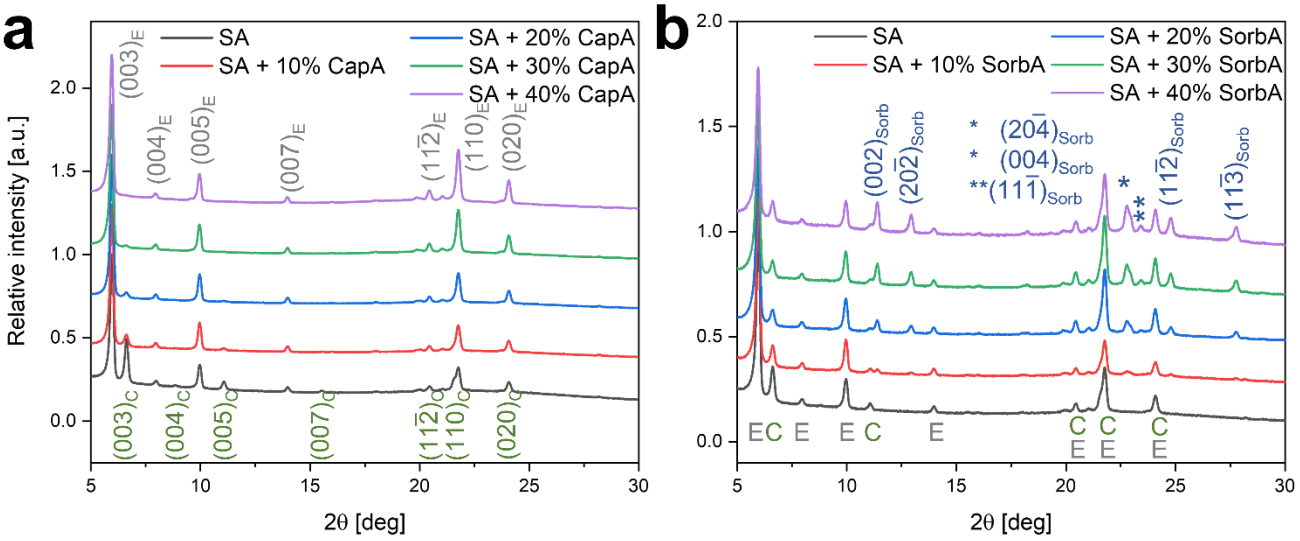


*Figure 2: XRD patterns of deposited coatings (λ = 1.54 Å). (a) Stearic acid coatings with 0% (control), 10%, 20%, 30%, and 40% caprylic acid. Two polymorphs of stearic acid are identified: C-form (green, indexed "C") and E-form (grey, indexed "E"). (b) Stearic acid coatings with 0% (control), 10%, 20%, 30%, and 40% sorbic acid. Stearic acid diffraction peaks are marked with "E" and "C" (indexed as in Fig. 1a), with additional diffraction peaks attributed to the sorbic acid phase, marked in blue ("Sorb").*

The collected X-ray diffraction patterns are shown in Figure 2. Analysis of the pure stearic acid coating (Figure 2a and 2b, black line) reveals the presence of two polymorphs of stearic acid: the C-form, which also exists in the original powdered material (SI 5), and the E-form, which emerges as a result of the spray deposition process. Both structures are bilayers composed of two molecules, with the carbon chains in an all-trans conformation.[63] The C-form is the high-temperature phase, but once formed, it remains metastable at RT for at least 2 years.[63] Given that crystallization occurs during the spray process at relatively low temperatures, the dominant polymorph formed is the E-form rather than the C-form. A preferred orientation of the (00l) planes for both C and E forms is clearly observed in the pure stearic acid diffraction pattern, compared to powder diffraction or theoretical data for the different polymorphs (SI 5, CIF: C-form: 1263279, E-form: 1263283). Notably, the $(003)_E$ plane associated with the E-form exhibits higher intensity than the corresponding plane for the C-form. This difference suggests that the E-form is the predominant phase in the spray-deposited coating (Figure 2, black line), as the intensity of these peaks would be similar in a randomly oriented powder sample.

The addition of caprylic acid influences crystallization, stabilizing the E-form of stearic acid over the C-form. In Figure 2a, diffraction patterns show that the intensity of $(00l)_C$ peaks associated with the C-form decreases with increasing caprylic acid content. This is particularly evident from the diminishing $(003)_C$ peak and the corresponding rise in intensity of diffraction peaks related to the E-form, such as

$(003)_E$. This behavior suggests that caprylic acid molecules adsorb at specific crystallographic sites of the stearic acid nuclei, promoting the formation of the E-form polymorph (Figure 1 a-e). The analysis of the X-ray diffractions collected from the coatings composed of stearic and varying amounts of sorbic acid (Figure 2 b) indicates the presence of the three phases: sorbic acid and both E-form and C-form of stearic acid. The intensity of the sorbic acid diffraction peaks increases with its increased amount in the formulation. Unlike the caprylic acid, sorbic acid promotes the formation of both the E- and C-form of stearic acid. This difference could be explained by the varying physical states of the MCFAs at RT. Caprylic acid, being liquid, adsorbs onto various facets of the formed stearic acid crystals affecting the crystallization process and causing a change in the growth rate of either E-form or C-form nuclei types. Sorbic acid, solid at RT, undergoes crystallization alongside the stearic acid crystals, therefore their effect on stearic acid crystallization is minimal. The XRD analysis of the coatings after 2 months of storage reveals minor structural changes, including the appearance of a peak at approximately 5.6°. This peak does not align with the known polymorphs of stearic acid according to existing literature but may indicate the onset of transformation and crystal reorganization. This new peak is most pronounced in pure stearic acid coatings, while the addition of caprylic and sorbic acids reduces its formation (SI 3 k, l).

High-resolution powder X-ray diffraction (HR-PXRD) using synchrotron radiation (λ = 0.354 Å) was employed to investigate whether the added MCFA molecules are incorporated into the stearic acid crystal lattice. Incorporation of these molecules alters the d-spaces within the lattice, resulting in peak shifts according to Bragg's law.[64] After applying a standard spraying procedure to coat glass substrates with various formulations, the coatings were mechanically detached from the substrate and analyzed in powdered form. The X-ray diffraction patterns of these powdered coatings are shown in SI 6.

The high-resolution diffraction patterns of the powdered coatings composed of stearic and caprylic acid mixtures corroborate the XRD data collected from the corresponding intact coatings presented in Figure 2, namely the presence of the two polymorphs of stearic acid where addition of caprylic acid favors the formation of the E-form over the C-form (SI 6 a, d). The main reflections of stearic acid that were found in the intact coatings are the $(00l)_E$, while $(003)_E$ is the strongest reflection therefore it was chosen as a representative peak of this direction, and the $(110)_E$ reflection, which is related to a different crystallographic direction. The further analysis was focused on these two reflections of stearic acid, as inter-lattice incorporation (of MCFA) leads to shifts of the reflections related to the matrix (stearic acid). A detailed analysis of the high-resolution diffractograms revealed that in the presence of both caprylic or sorbic acid, no shift in the position of the $(003)_E$ diffraction peak is observed (SI 6 b, e). In the case of caprylic acid addition, a slight shift of the $(110)_E$ peak to a lower d-

spacing is observed, indicating that a minimal inclusion of caprylic acid molecules into the lattice along the direction of stearic acid molecules may takes place (SI 6 c). Since the diffraction peak shift is only 0.0035º, corresponding to a 0.07% change in d-spacings, and this shift does not increase as the caprylic acid content rises from 20% to 30%, it can be concluded that the majority of the caprylic acid does not get incorporated within the stearic acid crystals. We would like to emphasize that such small shifts in the diffraction peaks have been demonstrated in other hybrid systems to result from intracrystalline incorporation, such as the inclusion of organic molecules within crystalline calcium carbonate.[64–67] An analysis of the $(003)_E$ peak reveals that the domain size (the average distance between defects) increased by 20%-40% with the addition of caprylic acid, indicating a significant increase in the average stearic acid crystal size. This increase may further explain the observed rise in roughness for the caprylic acid-containing samples (details in the discussion following SI 6). In the case of the sorbic acid addition, a similar shift in the $(110)_E$ peak is observed only for the sample with 10% sorbic acid but not at higher concentrations (SI 6 f). This can be explained by the fact that at low concentrations, sorbic acid is incorporated into the crystalline lattice of stearic acid, whereas at higher concentrations, when the solubility limit is likely exceeded, it segregates as separate crystals.

***Application of the coatings onto cellulose filter paper***

In the next step, the feasibility of coating flexible, porous substrates was investigated using cellulose filter paper (Whatman, grade 1, 25 mm, China) as a model surface. Cellulose-based materials, such as paper and wood, are highly susceptible to fungal contamination due to their hygroscopic nature. [68] Given that superhydrophobic surfaces are well known for their antimicrobial properties, coating compositions with the highest contact angles and the lowest potential release of MCFAs were selected for this experiment. Specifically, the pure stearic acid coating, along with stearic acid coatings containing 10% caprylic acid or 10% sorbic acid, were chosen. These compositions were sprayed on the paper, and the resulting coatings were characterized for their structure and wetting properties.

Figure 3c presents the confocal micrographs of the coated surfaces, revealing an increased roughness in comparison to the uncoated paper. While the neat uncoated paper, with a characteristic fibrous structure, exhibits roughness (Sq) of ~10 µm (Figure 3 a, c1, SI 7 a1), the coated papers display higher roughness of ~15-17 µm. This is observed for all three studied compositions and is ascribed to the contribution of the fatty acid crystals to the original roughness derived from the uncoated fibers (Figure 3 a, c2-c4, SI 7 a2-a4).

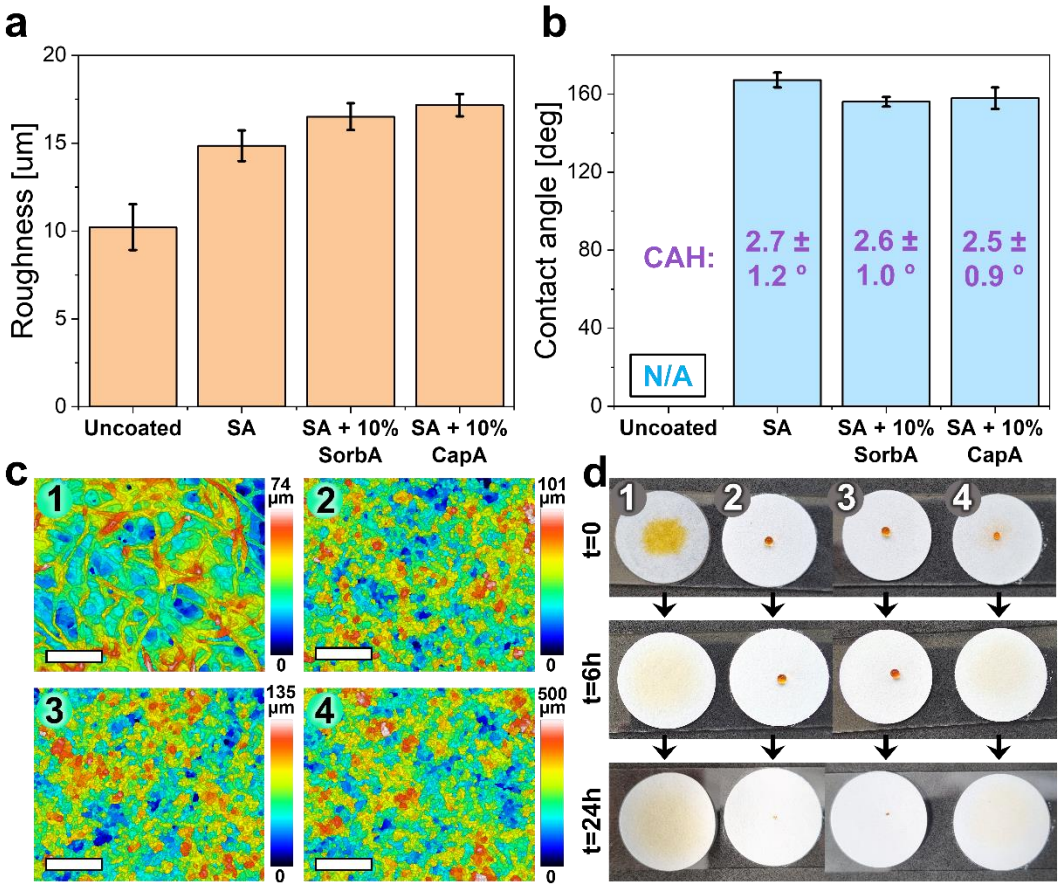


*Figure 3: Characterization of fatty acid-based coatings deposited on filter paper. (a) Roughness values. (b) Water contact angles. Values in purple display corresponding contact angle hysteresis. (c) Confocal microscope images of the uncoated and coated paper surfaces: (c1) Uncoated paper, (c2) Stearic acid coating, (c3) Stearic with 10% sorbic acid coating, (c4) Stearic with 10% caprylic acid coating. Scalebar is 200 µm. (d) Digital images of methyl orange-stained water droplets on wet filter papers with different coatings over time: (1) Uncoated paper (control), (2) Stearic acid coating, (3) Stearic + 10% sorbic acid coating, (4) Stearic + 10% caprylic acid coating.*

In all the three cases, the coating imparts superhydrophobic properties with self-cleaning ability to the paper surface (CA > 156$^{o}$ and CAH < 3$^{o}$) (Figure 3 b). To demonstrate the long-term superhydrophobic behavior of the coatings on a water-absorbing substrate, a 7 µL water droplet colored with methyl orange (for easier observation) was placed above the paper substrates. Digital images of the samples, shown in SI 7, indicate well-maintained superhydrophobicity over time in the case of both stearic acid and stearic acid with 10% sorbic acid coatings. Stearic acid with 10% caprylic acid coating exhibits short-term superhydrophobicity, followed by partial absorbance of the water droplet (SI 7 b2). The same experiment was performed using a moist paper to subject the coatings to challenging water exposure (see details in Experimental section), and the wetting properties of the coatings were monitored over time. As shown in Figure 3d, for both stearic acid and stearic acid with 10% sorbic acid coatings, the stained droplets remained unabsorbed even after 6 hours, indicating that these coatings prevent water penetration and remain superhydrophobic. After the water evaporated, the residual orange stain, caused by the low contact area between the droplet and the

coating, confirmed the stability of the superhydrophobic behavior (Figure 3 d, t=24h)). However, despite the initial superhydrophobic behavior of the stearic acid with 10% caprylic acid coating (SI 7 b1), partial droplet absorption was observed on the moist substrate, even at t=0 (Figure 3 d). The higher solubility of caprylic acid, combined with its oily nature that promotes a more homogeneous distribution among the stearic acid crystals, results in reduced coating durability.

***Leaching of MCFAs from the coatings***

The water contact angle values and morphology of the various coatings, as well as the changes in these characteristics over time under ambient conditions, are presented in Figure 1. The wetting properties of the sorbic acid-containing coatings remained stable over time (Figure 1f), whereas those of the caprylic acid-containing coatings changed progressively (Figure 1n), likely due to the gradual release of caprylic acid. The melting point of caprylic acid is significantly lower than that of sorbic acid ($T_{m\,(stearic\ acid)}$=67-69.6 °C, $T_{m\,(caprylic\ acid)}$= 16.3-16.7 °C, $T_{m\,(sorbic\ acid)}$= 132.8-134.6 °C).[69,70] This lower melting point leads to much faster diffusion of caprylic acid, which is trapped between stearic acid crystals, to the surface, where it can be released into the atmosphere. Consequently, we investigated the leaching behavior of MCFAs from the coatings.

To this end, the samples were immersed in water at ambient conditions for varying durations to accelerate the MCFAs leaching from the coatings. We note that, due to the significantly higher solubility of both caprylic and sorbic acids in water compared to stearic acid, their release into the aqueous medium is considerably greater over the duration of the experiment. (stearic acid: $2.9 \cdot 10^{-4}$[%], caprylic acid: 0.068[%], sorbic acid: 0.16[%])[71,72]. Following immersion, the coated samples were retrieved for characterization, and the composition of the residual aqueous medium was analyzed spectrophotometrically. To facilitate the analysis and prevent rapid release caused by excessive MCFA, 20% MCFA samples were selected from the tested concentration range of 10%–40% as the minimum concentration that induced significant changes in both morphology and wetting properties.

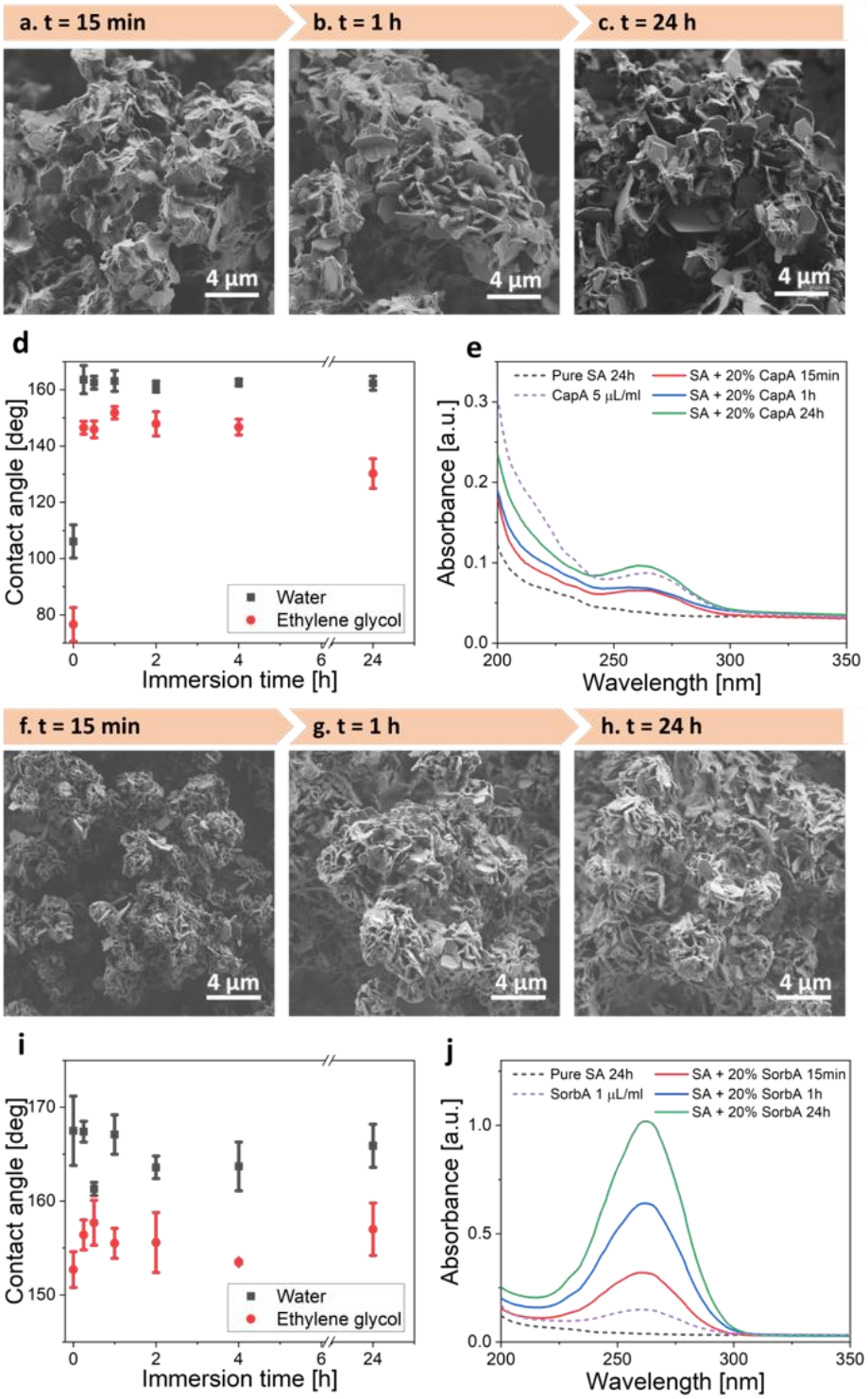


*Figure 4: (a-c) HR-SEM images of the coating composed of stearic acid and 20% caprylic acid following immersion in water for: (a) 15 min. (b) 1 h. (c) 24 h. (d) Changes in water (black) and ethylene glycol (red) contact angle values vs. immersion duration. (e) Corresponding absorbance spectra of the collected residual aqueous media following incubation. (f-h) HR-SEM images of the coating composed of stearic acid and 20% sorbic acid following immersion in water: (f) 15 min. (g) 1 h. (h) 24 h. (i) Changes in water (black) and ethylene glycol (red) contact angle values vs. immersion duration. (j) Corresponding absorbance spectra of the collected aqueous media following immersion.*

Figure 4 summarizes the characterization results for coatings composed of stearic acid with the addition of 20% caprylic or 20% sorbic acids after immersion in water for different time intervals. The surface morphology evolution of the stearic acid coating with 20% caprylic acid is shown in Figure 4 a-c. With increasing immersion time, more plate-like crystals emerge from the smooth fatty acid aggregates, leading to the development of a more pronounced hierarchical morphology, similar to that observed in pure stearic acid coatings. Correspondingly, the water contact angle increases from 106° to 163° within the first 15 minutes of immersion and remains stable upon longer immersion time, up to 24 hours (Figure 4 d). To confirm the release of caprylic acid, the coating was retrieved, and the composition of the residual aqueous medium was analyzed by absorbance measurements. The characteristic absorption peak of caprylic acid at 265 nm is detected for the caprylic acid-containing samples, with its intensity increasing as the immersion time progresses (Figure 4 e). These findings support the hypothesis that shorter, more water-soluble fatty acids leach out of the stearic acid matrix, facilitating the observed increase in the contact angle. The continued rise in the absorption peak intensity of caprylic acid over time further indicates ongoing release, even after the superhydrophobic contact angle stabilizes (after 15 minutes of immersion).

In the case of the stearic acid coating with 20% sorbic acid, the change in crystal morphology upon immersion in water is minimal, consistent with the minor influence of sorbic acid on the stearic acid coating under ambient conditions (Figure 4 f-h). The water and ethylene glycol contact angles measured on the post-immersion coatings remain constant within statistical error, even after 24 hours. However, similar to the stearic and caprylic acid system, the characteristic absorbance peak of sorbic acid at $\lambda$ = 265 nm is detected in the water after just 15 minutes of immersion. The peak intensity increases with immersion time, indicating a gradual release of sorbic acid into the surrounding aqueous medium. This release is further supported by XRD data, which show the disappearance of diffraction peaks associated with sorbic acid after immersion (SI 8 b).

However, the surrounding medium influences the kinetics of surface-related processes, and the aqueous environment likely facilitates the leaching of MCFAs from the coating. To conclusively demonstrate the release of caprylic acid under ambient conditions, two additional experiments were conducted. First, TGA analysis was performed in air environment on the coatings under slightly accelerated conditions at a temperature of 45°C. Second, the aqueous medium from the immersion experiments, corresponding to samples stored at ambient conditions for various durations, was analyzed using absorbance spectroscopy. Both experiments conclusively support the release of caprylic acid from the coating, even in the absence of an aqueous medium (see details in SI 9).

***Antifungal studies***

The antifungal activity of the developed single- and multi-component fatty acid coatings was studied against *Botrytis cinerea (B. cinerea*), known as gray mold. In these studies, *B. cinerea* mycelial plugs were positioned onto the coated cellulose filter papers (Figure 6a), and mycelium growth was quantified after 72 h.

All coated samples exhibited inhibited mycelial growth in comparison to the uncoated paper (Figure 5 a1-a4). We first examined mycelial growth on top of the paper and for the stearic acid-coated sample, a decrease of >60% in mycelial growth area is detected in comparison to the uncoated sample (Figure 5b, orange bars). Upon the addition MCFAs, this behavior is further intensified and coatings containing 10% caprylic acid were found to completely inhibit *B. cinerea* growth. Characterization of the coatings by optical microscopy (Figure 5 c1-c4) further supports these visual observations, and also indicates a decrease in the mycelial density developed on the surface of all coatings, where no mycelium was observed for the caprylic acid-containing coating.

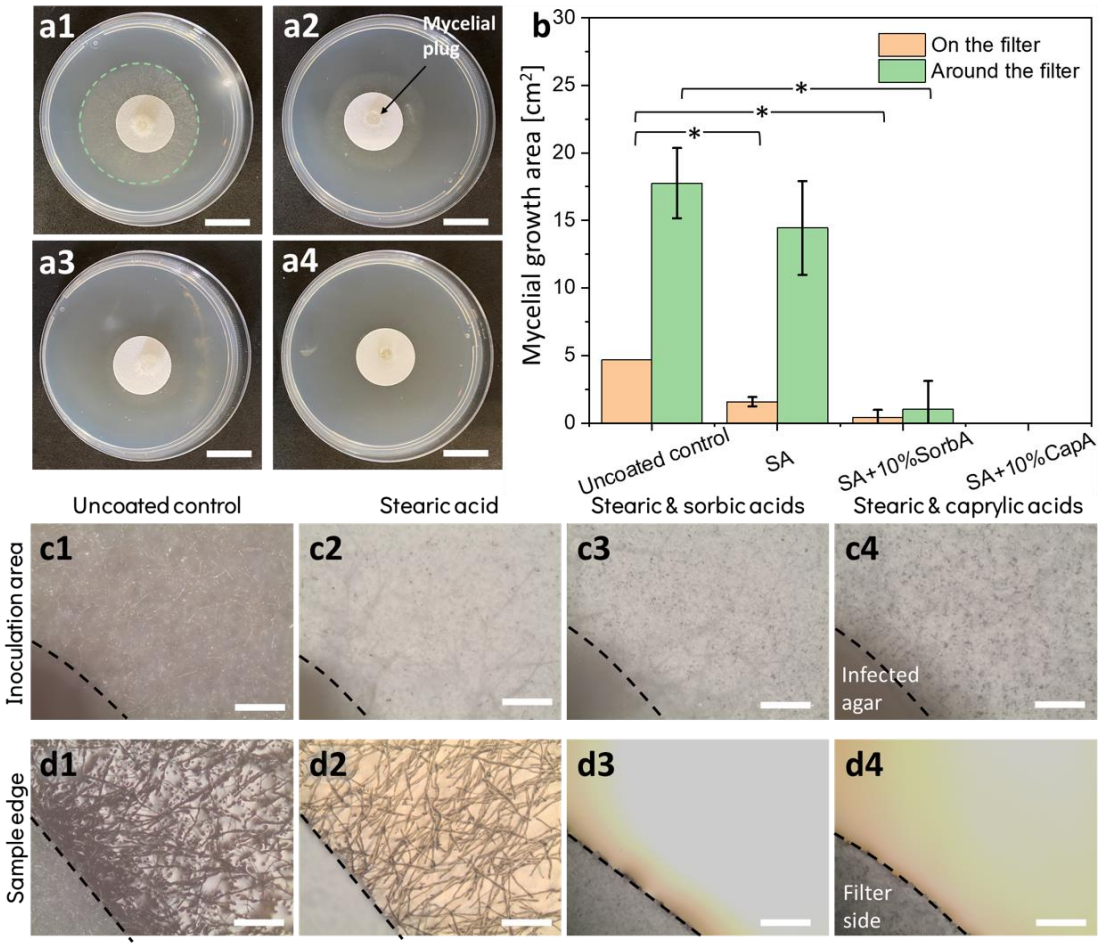


*Figure 5: Antifungal activity of fatty acid superhydrophobic coatings. (a) Digital images showing the mycelial growth of B. cinerea on coated papers: (a1) Uncoated paper (control, the mycelial growth on the agar is marked for clarity), (a2) Stearic acid coating, (a3) Stearic with 10% sorbic acid coating, (a4) Stearic with 10% caprylic acid coating. Scalebar: 2 cm. (b) Measured mycelial growth area values for coated and uncoated paper. (*) indicates significant difference (p-value ≤ 0.05) according to one-way ANOVA. (c1-c4) Optical microscope images of the mycelial plug area on uncoated control and coated samples (the mycelial plug edges are marked for clarity). Scalebar: 500 µm. (d1-d4) Optical microscope images of the paper edge at the interface with the PDA agar for coated and uncoated samples (the paper edge is marked for clarity). Scalebar: 500 µm.*

A similar inhibitory behavior is also observed when inspecting the PDA agar surrounding the paper. The addition of 10% MCFAs is found to significantly inhibit mycelial growth for sorbic acid and completely eradicate the fungi in the case of caprylic acid (

Figure 5 b-green bars, d1, d3-d4). This intensified growth inhibition effect on the top and around the samples containing MCFAs is expected and attributed to their intrinsic antifungal properties (see details in SI 10), and their diffusion to the surrounding agar upon the ability of the coating to release them. However, powdered stearic acid did not lead to any growth inhibition (SI 10 b) and yet, in the form of superhydrophobic coating it significantly prevented *B. cinerea* growth. The growth inhibition is well-observed on top of the coated paper (

Figure 5 b-orange bars, c1-c2). Moreover, the density of the mycelium network and the number of infection cushions[73] are reduced when comparing the morphology of the mycelium surrounding the stearic-acid coating to that developed around the uncoated paper (

Figure 5 d1-d2), despite the lack of intrinsic activity of stearic acid in a powder form (SI 10 b).

Electron microscopy was used to further investigate the morphology changes of the mycelium structures developed onto the coatings. Figure 6 b1 reveals that the mycelium growing on top of the stearic acid-coated sample present fewer hyphae in comparison to the dense well-branched network which developed onto the uncoated paper (Figure 6 a1). The hyphae are observed to extend between the stearic acid crystals and display a lower degree of invasive hyphal apical branching, limiting its ability to spread and colonize.[74,75] This behavior is also observed in the case of the stearic acid coating containing 10% sorbic acid, where sporadic entangled hyphae are detected (Figure 6 c1). No growth of *B. cinerea* was observed in the case of 10% caprylic acid containing coatings, in agreement with the optical microscopy results.

To investigate the effect of the coatings on the fungi viability, the samples were stained with FUN-1, a membrane-permeable fluorescent dye[61], and subsequently imaged. While the dye is internalized by both living and dead cells with intact plasma membranes, resulting in a diffuse green fluorescence within the cytoplasm, only in metabolically active cells, green fluorescence is converted into red cylindrical intracellular structures (CIVS) providing an indicator of cell viability.[58] Figure 6 a2-a3 depicts CLSM images of the uncoated paper, where the fungus is observed to produce abundant and well-formed hyphae in which numerous red CIVS are detected, confirming fungal viability. In the case of both stearic acid and stearic acid with 10% sorbic acid coatings (Figure 6 b2-b3, c2-c3), fewer CIVS are observed indicating a significant reduction in metabolic activity and fungal viability.[76] For the coating containing 10% caprylic acid, no fluorescence is detected (Figure 6 d2-d3) which is agreement with both optical and electron microscopy studies.

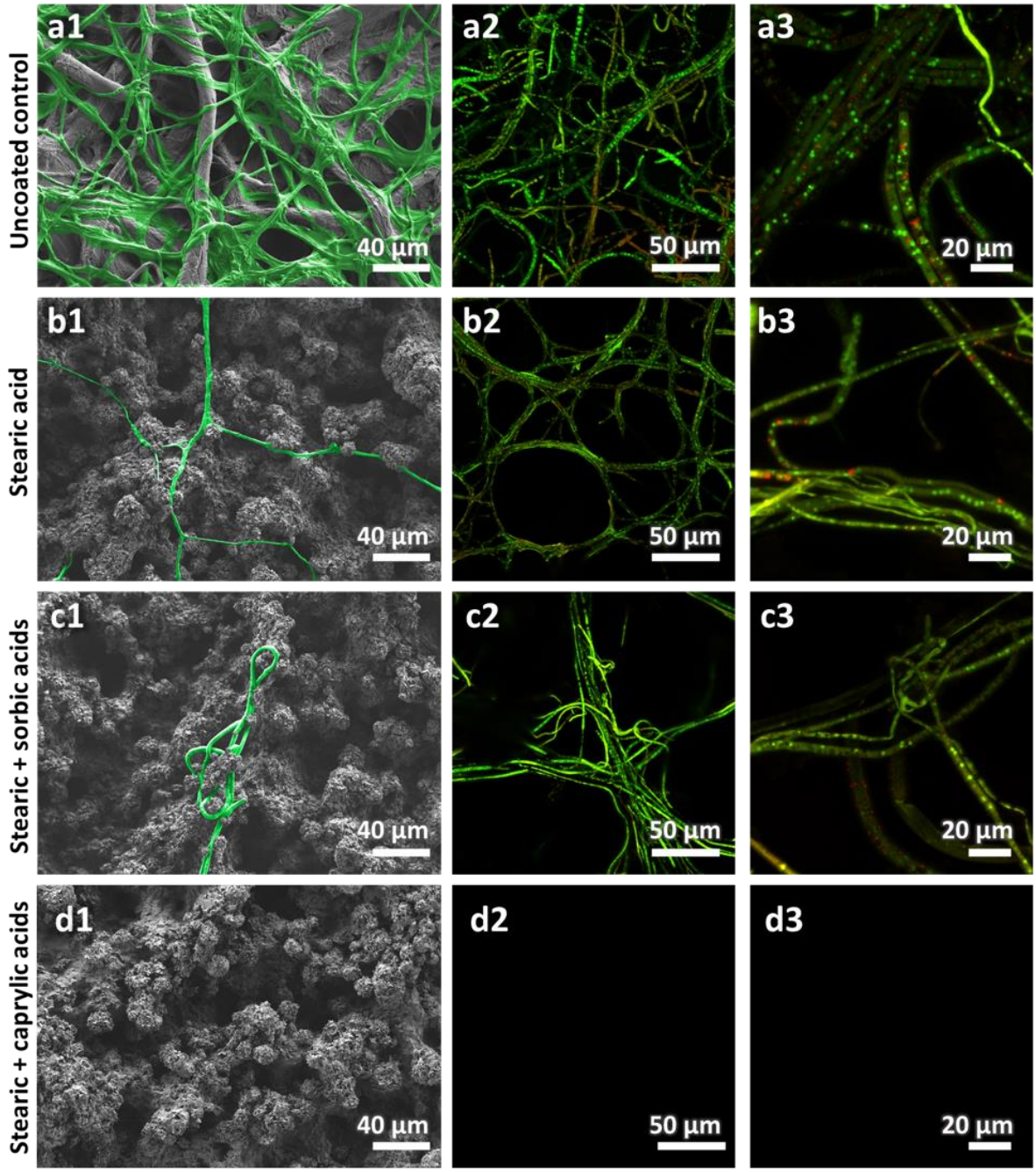


*Figure 6: Showcases microscopy images of B. cinerea that developed on the paper substrate after 72 hours of incubation at 24°C. (a1-d1) HR-SEM micrographs depict B. cinerea grown on uncoated paper, stearic acid-coated paper, stearic with 10% sorbic acid-coated paper, and stearic with 10% caprylic acid-coated paper, respectively. The mycelium is false-colored green for clarity. (a2-d2) LSCM images show B. cinerea stained with FUN-1 dye on the same corresponding papers. (a3-d3) Zoomed-in LSCM images present a closer look at B. cinerea after Fun-1 staining on the different coatings.*

These results demonstrate that the antifungal activity of the coatings can be tuned from passive inhibition of fungal adhesion and colonization onto the surface in the case of pure stearic acid coatings to biocidal in the case of MCFAs addition to the coatings, where complete eradication of the fungus can be realized. Superhydrophobic surfaces are well known for their antibiofouling properties,

particularly against bacteria.[14,77] In most cases, the surface's roughness minimizes the contact area available for pathogen cells, thereby reducing their adhesion and colonization. In our previous study we have demonstrated that superhydrophobic coatings based on single fatty acids, such as stearic acid, exhibit a unique combination of anti-biofouling and antibacterial properties against common bacteria.[33] The coating's selective activity against different bacteria is ascribed to their complex hierarchal structure and the fatty acid's intrinsic biocidal effect.[35] In this study, the MCFAs act as an active biocidal agents (SI 10 c-d) that are incorporated into superhydrophobic stearic acid the coating, which express its own passive antifungal behavior. These results agree with previous studies in which the antimicrobial properties of the studied MCFAs against numerous fungal species were demonstrated, as well as towards *B. cinerea.*[47,78] The antifungal properties of fatty acids are primarily attributed to their ability to partition within the lipid bilayer of the fungal membranes, increase their fluidity, and hence disrupt their integrity and function.[47] In addition, the antimicrobial action is also exerted by targeting various cellular functions, such as inhibition of topoisomerase, accumulation of reactive oxygen species, and interfering with fatty acids biosynthesis.[47] However, the limited amount of MCFAs in the coating and their gradual leaching are expected to provide only a short-term antifungal effect, whereas the pure stearic acid superhydrophobic coating acts passively, with its effectiveness not relying on the incorporation of potent MCFAs. Furthermore, in certain cases, an antifungal effect based on a passive mode of action, without the release of active compounds, may be advantageous. In such scenarios, the single-component stearic acid coating could effectively meet this requirement.

We propose that the superhydrophobicity and the multiscale topography of the stearic acid-based coatings are not only unfavorable for the adhesion of fungal spores but also disrupts the formation of stable *B. cinerea* mycelium.[79–81] This disruption leads to significant growth inhibition and notable alterations in mycelium morphology, particularly a reduced degree of branching. This reduction in branching adversely affects nutrient uptake and oxygen consumption, further impeding fungal growth.[75] Given that proper hyphal branching is crucial for the pathogenicity of *B. cinerea*, the observed decrease in branching may also account for diminished virulence and reduced colonization capacity.[74] When 10% of caprylic or sorbic acids are incorporated within the stearic acid coating, the hierarchical morphology and superhydrophobicity of the coatings are generally preserved. These potent MCFAs gradually leach out into the surrounding environment, exerting their antifungal effects through the mechanisms discussed earlier.[48] This in turn results in reduced fungal viability in the case of sorbic acid and complete *B. cinerea* inhibition for caprylic acid. Indeed, numerous studies have reported the superior antifungal activity, including fungicidal effects, of free caprylic acid against various types of filamentous fungi.[81,82] To summarize, the proposed superhydrophobic single-

component stearic acid coating can be used for passive prevention of fungal growth, while the initial antifungal effect can be intensified with an addition of potent MCFAs.

## Conclusions

In this study, we developed multifunctional superhydrophobic coatings composed of fatty acids with the capability to release active ingredients. These stearic acid coatings demonstrate excellent superhydrophobicity and self-cleaning abilities, even when incorporating water-soluble sorbic acid. They can be applied to various substrates, including flat glass and water-absorbing cellulose rough paper with complex fiber-like morphology, and remain durable even on fully wet substrates. We investigated the incorporation of MCFAs with varying chemical and physical properties into the coating and examined how the properties of the coating are affected when using solid or liquid fatty acids. Sorbic acid (solid) can be added in higher amounts with minimal impact on the coating's properties, whereas caprylic acid (liquid) significantly reduces superhydrophobicity and alters the morphology of the coatings. We demonstrated that the incorporated MCFAs can diffuse out of the stearic acid matrix, making them available as free compounds in the surrounding environment. The leaching out rate is environment-dependent, with accelerated release in aqueous conditions. Notably, as caprylic acid is released from the matrix, its influence on the coating properties diminishes, allowing the recovery of the coating's superhydrophobic characteristics.

The antifungal activity of the sprayed fatty acid coatings against *B. cinerea* was demonstrated for all studied formulations, including the pure stearic acid coating (without MCFAs). The incorporation of MCFAs further enhances the antifungal performance. The resulting coatings exhibit bi-modal functionality: a passive inhibitory effect provided by the superhydrophobic stearic acid coating, combined with the potent fungicidal action of the MCFAs embedded within the matrix. Thus, we suggest that while the leaching of caprylic acid provides an initial pronounced antifungal effect, the resulting increase in the coating's superhydrophobicity ensures sustained antifungal performance.

## Acknowledgments

The project has received funding from the Israeli Ministry of Innovation, Science and Technology.

We thank the European Synchrotron Radiation Facility (ESRF, Grenoble, France) for provision of synchrotron radiation facilities (beamline ID22).

We are indebted to the Lokey Interdisciplinary Center for Life Sciences and Engineering, Technion - Israel Institute of Technology for helping in setting up the CLSM studies.

We thank Prof. Alejandro Sosnik and Diana Solovyov for providing the facilities and assistance with absorbance measurements on Multiskan GO microplate spectrophotometer.

We thank Vitaly Prudnikov for false-coloring the HR-SEM images in Figure 6 to improve visualization. B.P. thanks the support of the Israel Discount Bank Academic Chair.

**References**

[1] W. Barthlott, M. Mail, C. Neinhuis, *Philos. Trans. R. Soc. A Math. Phys. Eng. Sci.* **2016**, *374*, 20160191.

[2] T. Darmanin, F. Guittard, *Mater. Today* **2015**, *18*, 273.

[3] H. K. Webb, R. J. Crawford, E. P. Ivanova, *Adv. Colloid Interface Sci.* **2014**, *210*, 58.

[4] B. B. Rich, B. Pokroy, *Soft Matter* **2018**, *14*, 7782.

[5] W. Barthlott, C. Neinhuis, *Planta* **1997**, *202*, 1.

[6] H. J. Ensikat, P. Ditsche-Kuru, C. Neinhuis, W. Barthlott, *Beilstein J. Nanotechnol.* **2011**, *2*, 152.

[7] B. Bhushan, Y. C. Jung, *Prog. Mater. Sci.* **2011**, *56*, 1.

[8] K. G. Krishnan, A. Milionis, E. Loth, T. E. Farrell, J. D. Crouch, D. H. Berry, *Appl. Surf. Sci.* **2017**, *392*, 723.

[9] B. Zhang, W. Xu, *New J. Chem.* **2021**, *45*, 15170.

[10] E. Vazirinasab, R. Jafari, G. Momen, *Surf. Coatings Technol.* **2018**, *341*, 40.

[11] X. Li, J. Yan, T. Yu, B. Zhang, *Colloids Surfaces A Physicochem. Eng. Asp.* **2022**, *642*, 128701.

[12] T. P. Rasitha, N. G. Krishna, B. Anandkumar, S. C. Vanithakumari, J. Philip, *Adv. Colloid Interface Sci.* **2024**, *324*, 103090.

[13] J. Jeevahan, M. Chandrasekaran, G. Britto Joseph, R. B. Durairaj, G. Mageshwaran, *J. Coatings Technol. Res.* **2018**, *15*, 231.

[14] D. Ashok, S. Cheeseman, Y. Wang, B. Funnell, S. F. Leung, A. Tricoli, D. Nisbet, *Adv. Mater. Interfaces* **2023**, *10*, 2300324.

[15] N. J. Shirtcliffe, G. McHale, S. Atherton, M. I. Newton, *Adv. Colloid Interface Sci.* **2010**, *161*, 124.

[16] M. Ma, R. M. Hill, *Curr. Opin. Colloid Interface Sci.* **2006**, *11*, 193.

[17] A. B. D. Cassie, S. Baxter, *Trans. Faraday Soc.* **1944**, *40*, 546.

[18] L. Feng, Y. Zhang, J. Xi, Y. Zhu, N. Wang, F. Xia, L. Jiang, *Langmuir* **2008**, *24*, 4114.

[19] J. B. K. Law, A. M. H. Ng, A. Y. He, H. Y. Low, *Langmuir* **2014**, *30*, 325.

[20] Y. Y. Yan, N. Gao, W. Barthlott, *Adv. Colloid Interface Sci.* **2011**, *169*, 80.

[21] T. Darmanin, E. T. De Givenchy, S. Amigoni, F. Guittard, *Adv. Mater.* **2013**, *25*, 1378.

[22] P. Kim, T.-S. Wong, J. Alvarenga, M. J. Kreder, W. E. Adorno-Martinez, J. Aizenberg, *ACS Nano* **2012**, *6*, 6569.

[23] S. Xu, Q. Wang, N. Wang, *Adv. Eng. Mater.* **2021**, *23*, 1.

[24] K. Manoharan, S. Bhattacharya, *J. Micromanufacturing* **2019**, *2*, 59.

[25] A. Hooda, M. S. Goyat, J. K. Pandey, A. Kumar, R. Gupta, *Prog. Org. Coatings* **2020**, *142*, 105557.

[26] T. S. Wong, S. H. Kang, S. K. Y. Tang, E. J. Smythe, B. D. Hatton, A. Grinthal, J. Aizenberg, *Nature* **2011**, *477*, 443.

[27] S. Pechook, B. Pokroy, *Adv. Funct. Mater.* **2012**, *22*, 745.

[28] S. Pechook, A. Katsman, B. Pokroy, *Cryst. Growth Des.* **2016**, *16*, 3932.

[29] S. Pechook, N. Kornblum, B. Pokroy, *Adv. Funct. Mater.* **2013**, *23*, 4572.

[30] S. Pechook, K. Sudakov, I. Polishchuk, I. Ostrov, V. Zakin, B. Pokroy, M. Shemesh, *J. Mater. Chem. B* **2015**, *3*, 1371.

[31] S. Pechook, B. Pokroy, *Soft Matter* **2013**, *9*, 5710.

[32] I. Ostrov, I. Polishchuk, M. Shemesh, B. Pokroy, *ACS Appl. Bio Mater.* **2019**, *2*, 4932.

[33] E. Prudnikov, I. Polishchuk, A. Sand, H. A. Hamad, N. Massad-Ivanir, E. Segal, B. Pokroy, *Mater. Today Bio* **2023**, *18*, 100516.

[34] A. P. Desbois, V. J. Smith, *Appl. Microbiol. Biotechnol.* **2010**, *85*, 1629.

[35] G. Casillas-Vargas, C. Ocasio-Malavé, S. Medina, C. Morales-Guzmán, R. G. Del Valle, N. M.

Carballeira, D. J. Sanabria-Ríos, *Prog. Lipid Res.* **2021**, *82*, 101093.

[36] E. P. Ivanova, S. H. Nguyen, Y. Guo, V. A. Baulin, H. K. Webb, V. K. Truong, J. V. Wandiyanto, C. J. Garvey, P. J. Mahon, D. E. Mainwaring, R. J. Crawford, *Acta Biomater.* **2017**, *59*, 148.

[37] V. B. Hoa, D. H. Song, K. H. Seol, S. M. Kang, H. W. Kim, J. H. Kim, S. H. Cho, *Meat Sci.* **2022**, *184*.

[38] N. V. Patil, A. N. Netravali, *Cellulose* **2020**, *27*, 545.

[39] A. Gayathri, M. G. Sethuraman, *Cellulose* **2024**, *31*, 1967.

[40] S. S. Cassidy, K. Page, C. I. D. L. Reyes, E. Allan, I. P. Parkin, C. J. Carmalt, *ACS Omega* **2024**, *9*, 7154.

[41] C. R. C. Diaz Brenda Resendiz, *Superhydrophobic Coating-Recent Adv. Theory Appl.* **2023**, *IntechOpen*.

[42] M. Mu, W. Zhou, Y. Arcot, L. Cisneros-Zevallos, M. Akbulut, *Food Packag. Shelf Life* **2024**, *43*, 101290.

[43] I. S. Bayer, *Adv. Mater. Interfaces* **2020**, *7*, 1.

[44] F. B. JD Stopforth, JN Sofos, *Sorbic acid and sorbates*, **2005**.

[45] M. Amin Zare, S. M. Razavi Rohani, M. Raeisi, S. H. Javadi Hosseini, M. Hashemi, *J. Food Qual. Hazards Control* **2014**, *1*, 52.

[46] M. K. M. Nair, J. Joy, P. Vasudevan, L. Hinckley, T. A. Hoagland, K. S. Venkitanarayanan, *J. Dairy Sci.* **2005**, *88*, 3488.

[47] C. H. Pohl, J. L. F. Kock, V. S. Thibane, *Sci. against Microb. Pathog. Curr. Res. Technol. Adv.* **2011**, *1*, 61.

[48] A. Guimarães, A. Venâncio, *Toxins (Basel).* **2022**, *14*, 1.

[49] D. Seidel, S. Wurster, J. D. Jenks, H. Sati, J. P. Gangneux, M. Egger, A. Alastruey-Izquierdo, N. P. Ford, A. Chowdhary, R. Sprute, O. Cornely, G. R. Thompson, M. Hoenigl, D. P. Kontoyiannis, *The Lancet Microbe* **2024**, *5*, e594.

[50] D. Simões, E. de Andrade, R. Sabino, *Encyclopedia* **2023**, *3*, 900.

[51] D. W. Denning, *Lancet Infect. Dis.* **2024**, *24*, e428.

[52] J. Xu, *mLife* **2022**, *1*, 223.

[53] P. H. Le, D. P. Linklater, A. A. Medina, S. MacLaughlin, R. J. Crawford, E. P. Ivanova, *Acta Biomater.* **2024**, *177*, 20.

[54] B. Williamson, B. Tudzynski, P. Tudzynski, J. A. L. Van Kan, *Mol. Plant Pathol.* **2007**, *8*, 561.

[55] G. Romanazzi, E. Feliziani, *Botrytis cinerea (Gray Mold)*, Elsevier, **2014**.

[56] M. A. Jacometti, S. D. Wratten, M. Walter, *Aust. J. Grape Wine Res.* **2010**, *16*, 154.

[57] N. Massad-Ivanir, A. Sand, N. Nitzan, E. Valderama, M. Kurczewski, H. Remde, A. Wegenberger, K. Shlosman, R. Shemesh, A. Störmer, E. Segal, *Food Packag. Shelf Life* **2023**, *37*, 1.

[58] B. D. Essary, P. A. Marshall, *J. Microbiol. Methods* **2009**, *78*, 208.

[59] S. Guillou, V. Besnard, N. El Murr, M. Federighi, *Int. J. Food Microbiol.* **2003**, *88*, 85.

[60] S. C. A. Chen, S. Patel, W. Meyer, B. Chapman, H. Yu, K. Byth, P. G. Middleton, H. Nevalainen, T. C. Sorrell, *Mycopathologia* **2018**, *183*, 251.

[61] J. Kraut-Cohen, O. Frenkel, S. Covo, E. Marcos-Hadad, S. Carmeli, E. Belausov, D. Minz, E. Cytryn, *Pest Manag. Sci.* **2024**, *80*, 2804.

[62] H. K. Webb, V. K. Truong, J. Hasan, C. Fluke, R. J. Crawford, E. P. Ivanova, *Scanning* **2012**, *34*, 257.

[63] E. Moreno-Calvo, G. Gbabode, R. Cordobilla, T. Calvet, M. À. Cuevas-Diarte, P. Negrier, D. Mondieig, *Chem. - A Eur. J.* **2009**, *15*, 13141.

[64] A. Lang, I. Polishchuk, G. Confalonieri, C. Dejoie, A. Maniv, D. Potashnikov, E. N. Caspi, B. Pokroy, *Adv. Mater.* **2022**, *34*.

[65] A. Lang, I. Polishchuk, A. Katsman, B. Pokroy, *Cryst. Growth Des.* **2023**, *23*, 5117.

[66] A. Lang, A. Brif, I. Polishchuk, A. N. Fitch, J. Feldmann, B. Pokroy, *Adv. Opt. Mater.* **2022**, *10*.

[67] S. Mijowska, I. Polishchuk, A. Lang, E. Seknazi, C. Dejoie, S. Fermani, G. Falini, N. Demitri, M. Polentarutti, A. Katsman, B. Pokroy, *Chem. Mater.* **2020**, *32*, 4205.

[68] A. A. Haleem Khan, S. Mohan Karuppayil, *Saudi J. Biol. Sci.* **2012**, *19*, 405.

[69] E. Tvrzicka, L.-S. Kremmyda, B. Stankova, A. Zak, *Biomed. Pap.* **2011**, *155*, 117.

[70] J. H. F. de Jesus, I. M. Szilágyi, G. Regdon, E. T. G. Cavalheiro, *Food Chem.* **2021**, *337*, 127770.

[71] E. Lück, M. Jager, *Antimicrob. Food Addit.* **1997**, 152.

[72] C. W. H. Ralston, A W, *J. Org. Chem.* **1942**, *7*, 546.

[73] X. Liu, J. Xie, Y. Fu, D. Jiang, T. Chen, J. Cheng, *Int. J. Mol. Sci.* **2020**, *21*.

[74] Y. Liu, J. K. Liu, G. H. Li, M. Z. Zhang, Y. Y. Zhang, Y. Y. Wang, J. Hou, S. Yang, J. Sun, Q. M. Qin, *Mol. Plant Pathol.* **2019**, *20*, 731.

[75] M. Papagianni, *Biotechnol. Adv.* **2004**, *22*, 189.

[76] K. A. Marr, M. Koudadoust, M. Black, S. A. Balajee, *Clin. Diagn. Lab. Immunol.* **2001**, *8*, 1240.

[77] J. Hasan, R. J. Crawford, E. P. Ivanova, *Trends Biotechnol.* **2013**, *31*, 295.

[78] R. Coleman, V. Yang, B. Woodward, C. Clausen, *106 Anu. Meet. Am. Wood Prot. Assoc.* **2010**.

[79] H. Fan, Z. Guo, *Biomater. Sci.* **2020**, *8*, 1502.

[80] A. Aburto-Medina, P. H. Le, S. MacLaughlin, E. Ivanova, *Appl. Microbiol. Biotechnol.* **2021**, *105*, 2663.

[81] D. P. Linklater, P. H. Le, A. Aburto-Medina, R. J. Crawford, S. Maclaughlin, S. Juodkazis, E. P. Ivanova, *Int. J. Mol. Sci.* **2023**, *24*, 1.

[82] S. Liu, W. Ruan, J. Li, H. Xu, J. Wang, Y. Gao, J. Wang, *Mycopathologia* **2008**, *166*, 93.

[83] K. F. Kelton, *Crystal Nucleation in Liquids and Glasses*, Vol. 45, **1991**.

**SI**

Composition of the solutions

The composition of solutions used to form various coatings is detailed in SI 1. The caprylic acid volume was calculated by division of the required weight (the same as for sorbic acid) by the density – 0.910 g/mL.

*SI 1: Composition of spray solutions used to form multi-component coatings*

| MCFA concentration in the coating [%] | Stearic acid weight in 50 mL of 0.02 g/ mL solution [g] | Sorbic acid weight (±5 mg) [mg] | Caprylic acid volume [µL] |
|---|---|---|---|
| 10 | 1 | 111 | 122.1 |
| 20 | 1 | 250 | 274.7 |
| 30 | 1 | 429 | 471.0 |
| 40 | 1 | 667 | 732.6 |

Roughness and surface parameters:

Root mean square values (Sq) shown in Figure 1 provide the information on vertical dimensions of the surface. For better understanding of the fabricated surfaces, roughness parameters addressing the horizontal surface dimensions[62], namely developed area ratio (Sdr, SI 2 a, d) and density of peaks (Spd, SI 2 b, e) were tested, as well as the skewness (Ssk), which is related to the histogram of height distribution of the scanned surface (SI 2 c, f). In both cases, coatings with caprylic or with sorbic acid, the Sdr and Spd values follow the same trend that shown for Sq: for higher roughness, also higher values of the developed area ratio and the peaks density were obtained. The sample with 10% caprylic acid expresses the same roughness value, but slightly higher Sdr and Spd values in comparison to the 20% caprylic acid. The higher values of the developed area ratio and the peaks density may be addressed to less prominent smoothing of the surface features that increase with the addition of

caprylic acid to the formulation. Low positive values of the skewness indicate relatively narrow surface features that formed on the supporting substrate.

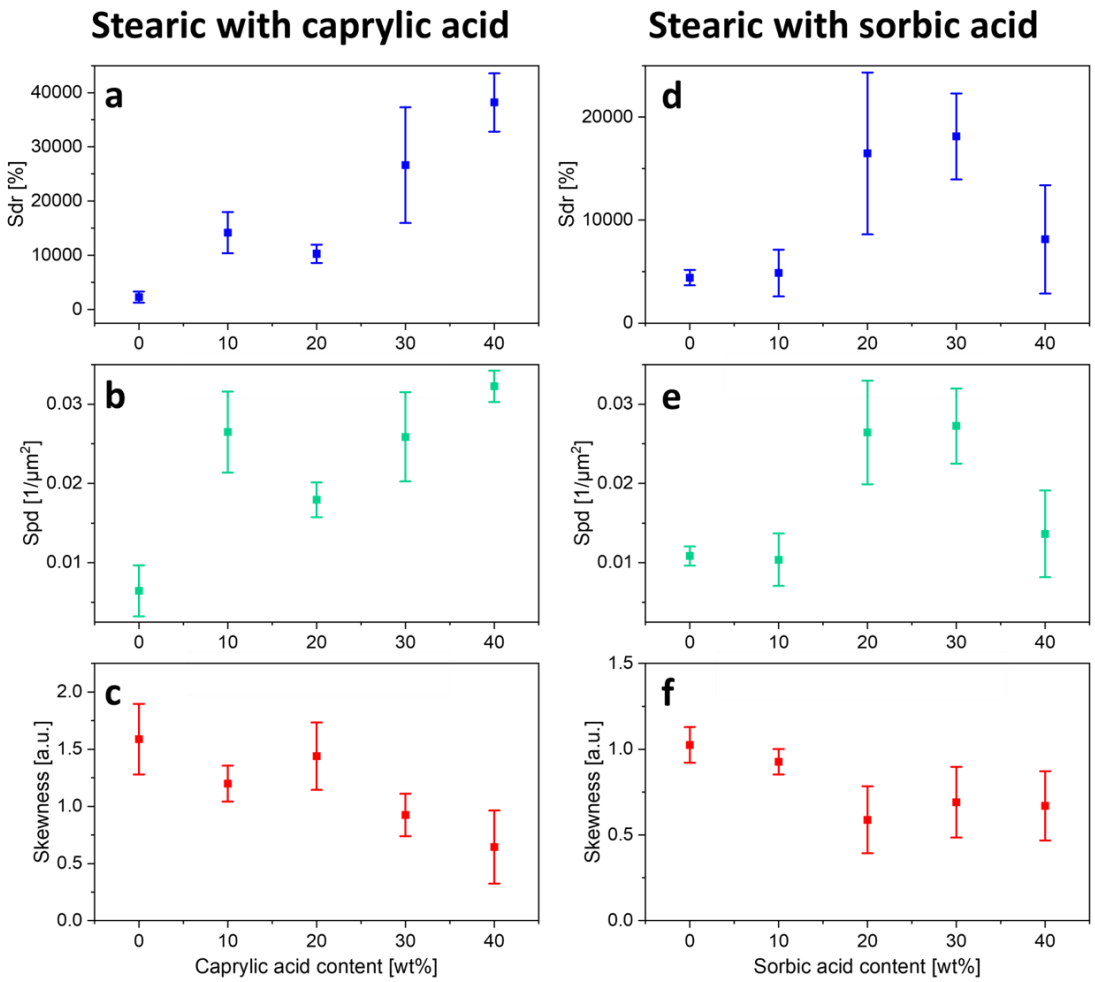


*SI 2: Roughness parameters derived from confocal microscope measurements. (a-c) Caprylic acid containing coatings, (d-f) Sorbic acid containing coatings. (a, d) Developed area ratio (Sdr), (b, e) Density of peaks (Spd), (c, f) Skewness (Ssk).*

2-months stability of the coatings:

HR-SEM images and X-ray diffractions of the coatings were obtained after 2 months of storage at ambient conditions. The results are shown in SI 3:

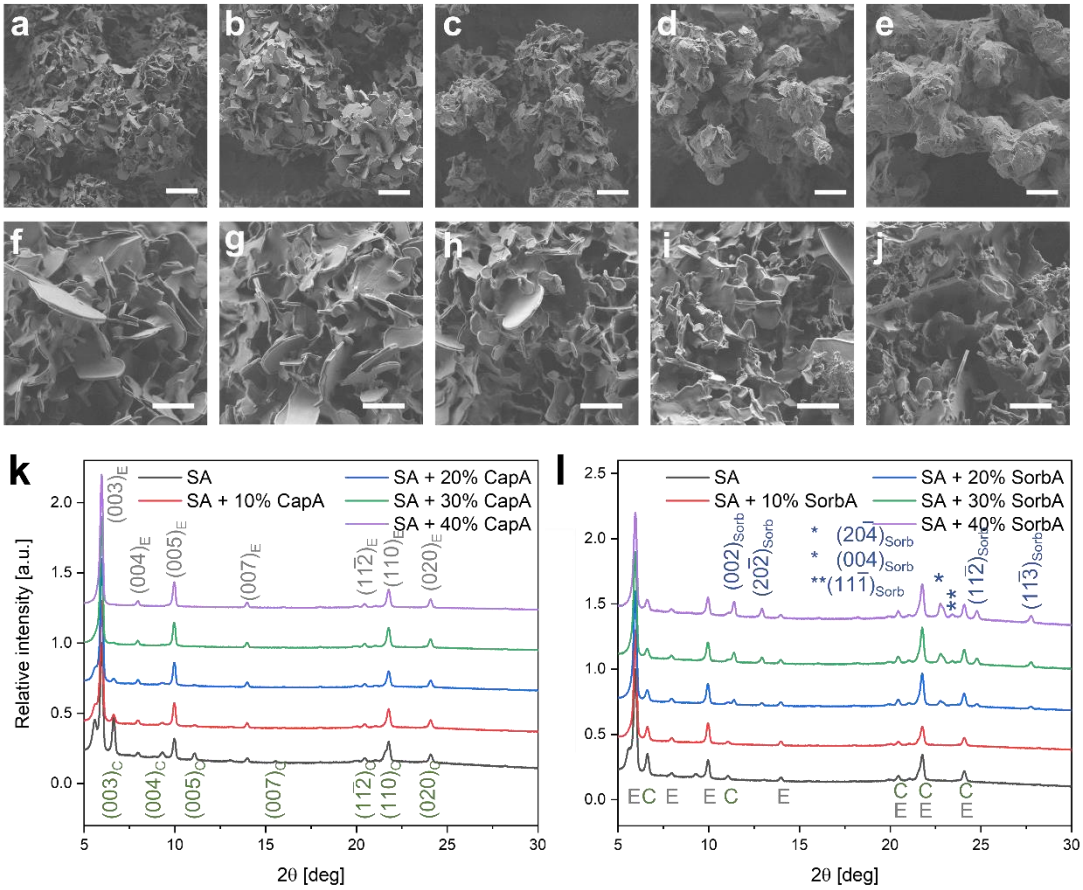


*SI 3: The coatings after 2 months of storage: (a-e) HR-SEM images of sprayed stearic acid coating with increasing amounts of caprylic acid – 0%, 10%, 20%, 30%, and 40% caprylic acid, respectively. Scalebar is 6 µm. (f-j) HR-SEM images of sprayed stearic acid coating with increasing amounts of sorbic acid – 0%, 10%, 20%, 30%, and 40% of sorbic acid, respectively, scalebar is 2 µm. (k) XRD of the stearic acid coatings with the addition of 0% (control), 10%, 20%, 30% and 40% of caprylic acid. (l) XRD of the stearic acid coatings with the addition of 0% (control), 10%, 20%, 30% and 40% of sorbic acid.*

Contrary to a significant change in the wetting properties of stearic with caprylic acid coatings over time (Figure 1 f-g), no significant morphological changes were found after two months of storage at ambient conditions (Figure 1 a-e vs. SI 3 a-e). The possible evaporation of caprylic acid from the surface improves the hydrophobicity due to the chemical change of the outer coating layer and causes an increase in the contact angle. Still, the formed crystals cannot be easily reorganized and the characteristic morphology of the pure sprayed stearic acid is not recovered. The morphology of the coatings formed from out of stearic with sorbic acid remains stable over the tested period (Figure 1 i-m vs. SI 3 f-j). The XRD of the coatings after 2 months of storage at ambient conditions for both coating series of stearic acid with caprylic or with sorbic acid does not show significant changes, except for an appearance of peak at ~5.6°. This peak does not accurately fit the polymorphs of stearic acid but may indicate the beginning of transformation and crystal reorganization. This new peak appearance is most

prominent in pure stearic acid coatings, and adding both caprylic and sorbic acids decreases its formation.

Wide FoV of stearic with sorbic acid coatings:

HR-SEM images of stearic with sorbic acid coatings at similar magnification as stearic with caprylic acid coatings shown in Figure 1 a-e:

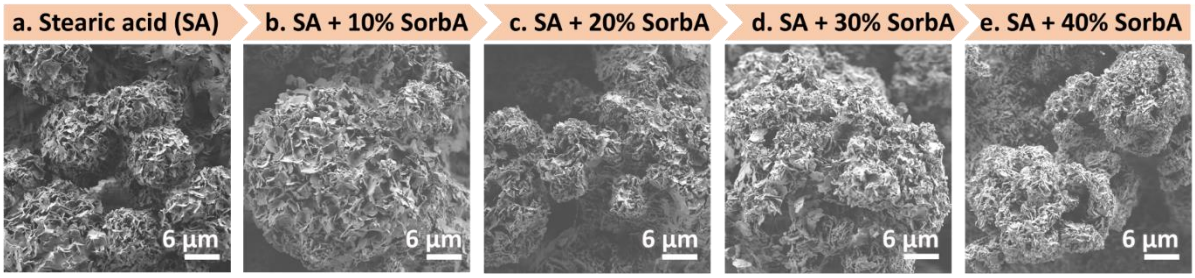


*SI 4: HR-SEM images of sprayed stearic acid coating with various amounts of sorbic acid (SorbA) – 0%, 10%, 20%, 30%, and 40%, respectively*

X-ray diffraction of powdered stearic acid:

SI 5 shows the diffraction patterns of powdered stearic acid and sprayed stearic acid coating. The spray processing results in a preferred orientation of the (00l) plane and a prefferable formation of the E-form polymorph.

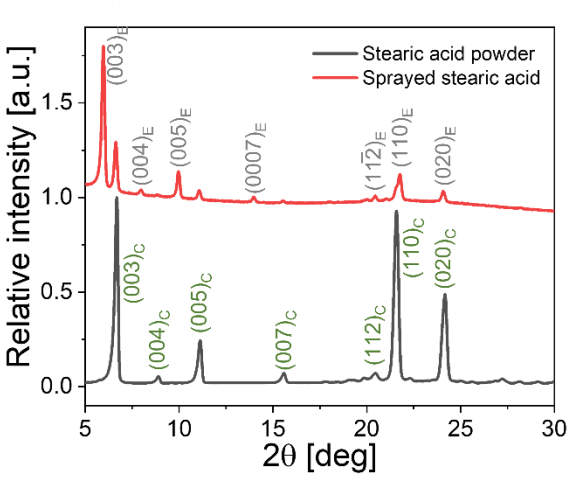


*SI 5: XRD of powdered stearic acid and stearic acid coating formed by spray coating.*

HR-PXRD of the powdered coatings:

The high-resolution diffractions of the powdered coatings (HR-PXRD) of stearic with caprylic acid coatings support the obtained data from the XRD of the intact coatings shown in Figure 2.

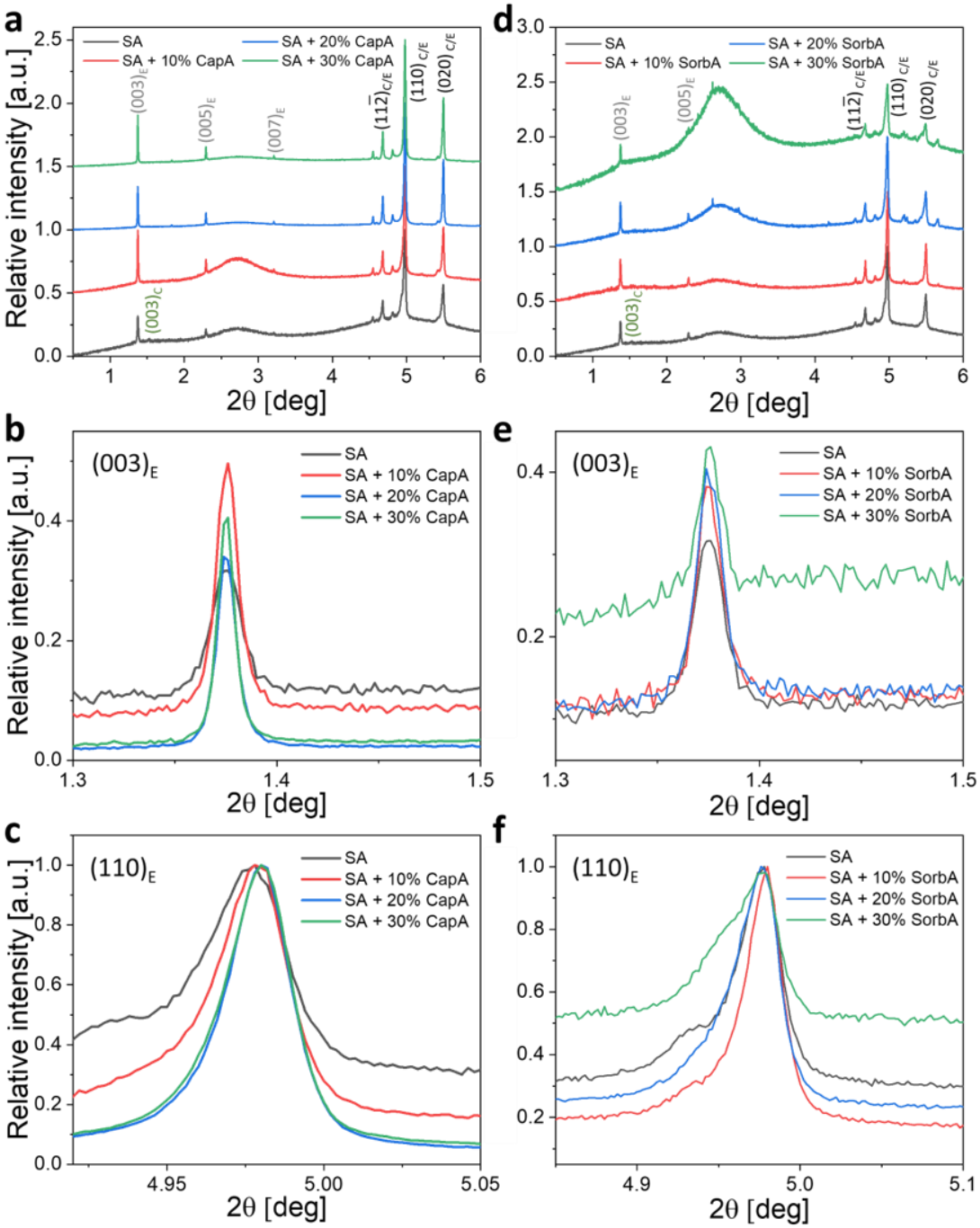


*SI 6: HR-PXRD of detached powdered coatings performed with λ=0.3542 [Å]: (a-c) Detached powdered coatings of stearic with caprylic acid. (a) Diffraction of 0.5-6 [deg] range. (b) Zoom-in on the $(003)_E$ reflection. (c) Zoom-in on the $(110)_E$ reflection. (d-f) Detached powdered coatings of stearic with sorbic acid. (d) Diffraction of 0.5-6 [deg] range. (e) Zoom-in on the $(003)_E$ reflection. (f) Zoom-in on the $(110)_E$ reflection.*

The increase in roughness of the caprylic acid containing samples may also be associated with an increase in the average size of stearic acid crystals, which is manifested in an increase in the average domain size (the distance between defects in the crystal lattice). The domain size was calculated according to Scherrer equation, when FWHM of the $(003)_E$ peak of stearic acid was analyzed (Figure SI 6 b):

$$\tau = \frac{K\lambda}{\beta \cos(\theta)} \quad (1S)$$

where τ is the mean size of the ordered (crystalline) domains, λ is the radiation wavelength (λ=0.3542Å for synchrotron radiation), β is the peak broadening at half the maximum (FWHM), and θ is the Bragg angle.

According to this analysis, the domain size increases in the caprylic acid containing samples by 20%-40%. Corresponding increase in the average size of stearic acid crystals can be explained by a decrease in the nucleation rate (*J*) of stearic acid crystals, when crystallization starts from a solution containing both stearic and caprylic acid:

$$J \sim \exp(-\Delta G / k_B T) \quad (2S)$$

where ΔG is the free energy barrier for nucleation, $k_B$ is the Boltzmann constant, $T$ is the absolute temperature; according to classical theory of nucleation[83]:

$$\Delta G = k\gamma^3 / \Delta G_v^2 \quad (3S)$$

where γ is the nucleus surface tension, $\Delta G_v$ is the Gibbs free energy change during solidification of stearic acid per unit volume, *k* is a dimensionless geometry factor. The $\Delta G_v$ represents the gain in free energy during the transition of stearic acid molecules from a liquid solution to a nucleated crystal of stearic acid, and equals to the difference between the free energy of the stearic acid molecules in the crystal, $\Delta G_v^{crys}$, and their free energy in the solution, $\Delta G_v^{sol}$:

$$\Delta G_v = \Delta G_v^{crys} - \Delta G_v^{sol} \quad (4S)$$

It should be noted that all these free energies are negative, and $\Delta G_v^{crys}$ is more negative than $\Delta G_v^{sol}$, which is the driving force for crystallization. It is quite reasonable to assume that the presence of caprylic acid molecules in the solution leads to decrease of the $\Delta G_v^{sol}$ (making it more negative) due

to substantial interaction of stearic and caprylic molecules present in the solvent - diethyl ether; interactions of stearic acid molecules with caprylic acid molecules is stronger than that with molecules of diethyl ether due to stronger hydrogen bonding (two carboxylic acids vs. one carboxylic acid in an ether) and due to additional hydrophobic interactions from the long alkyl chains of stearic and caprylic acid which contribute to van der Waals interactions. Decreasing $G_v^{sol}$ (and therefore increasing in absolute value) results in decrease of $\Delta G_v$, leading to increase of the free energy barrier for nucleation $\Delta G$, eq.(3S), and corresponding decrease of the nucleation rate, eq.(2S). It results finally in fewer stearic acid crystals of larger size. Since the final total number of crystals, $N$, is proportional to the nucleation rate, $J$, an average size of crystals can be estimated as:

$$\bar{D} = L / N^{1/3} \sim \exp\left(\frac{\Delta G}{3k_B T}\right) = \exp\left(\frac{k\gamma^3}{3\Delta G_v^2 k_B T}\right) , \qquad (5S)$$

where $L$ is the linear size of the solidified system. So, the average size increases exponentially with decrease of $\Delta G_v$. These larger (and in smaller number) crystals then participate in formation of smoother spheres, which is provided by liquid layers of caprylic acid. In contrast, spheres formed from the pure stearic acid solution are comprised of a high number of separate plate-like crystals.

Characterization of the coatings applied on cellulose filter paper:

The application feasibility and performance of the pure stearic acid coating and multi-component stearic acid coating containing 10% caprylic or 10% sorbic acid were tested when applied on filter paper and their HR-SEM images were obtained (SI 7 a1-a4). The coatings' morphology is similar to the obtained morphology when deposited on glass slides (Figure *1* a, b, I, j). Higher heterogeneity of crystal distribution can be seen as a result of the fiber-like substrate structure, supporting the obtained results from the dynamic confocal microscope scans (Figure 3 c).

To test the wetting properties of the coating when water-absorbing filter paper acts as a substrate, a methyl orange-colored water droplet of 7 µL was placed above the samples, covered with a petri dish to avoid evaporation, and followed over time. The results are shown in SI 7 b1-b3:

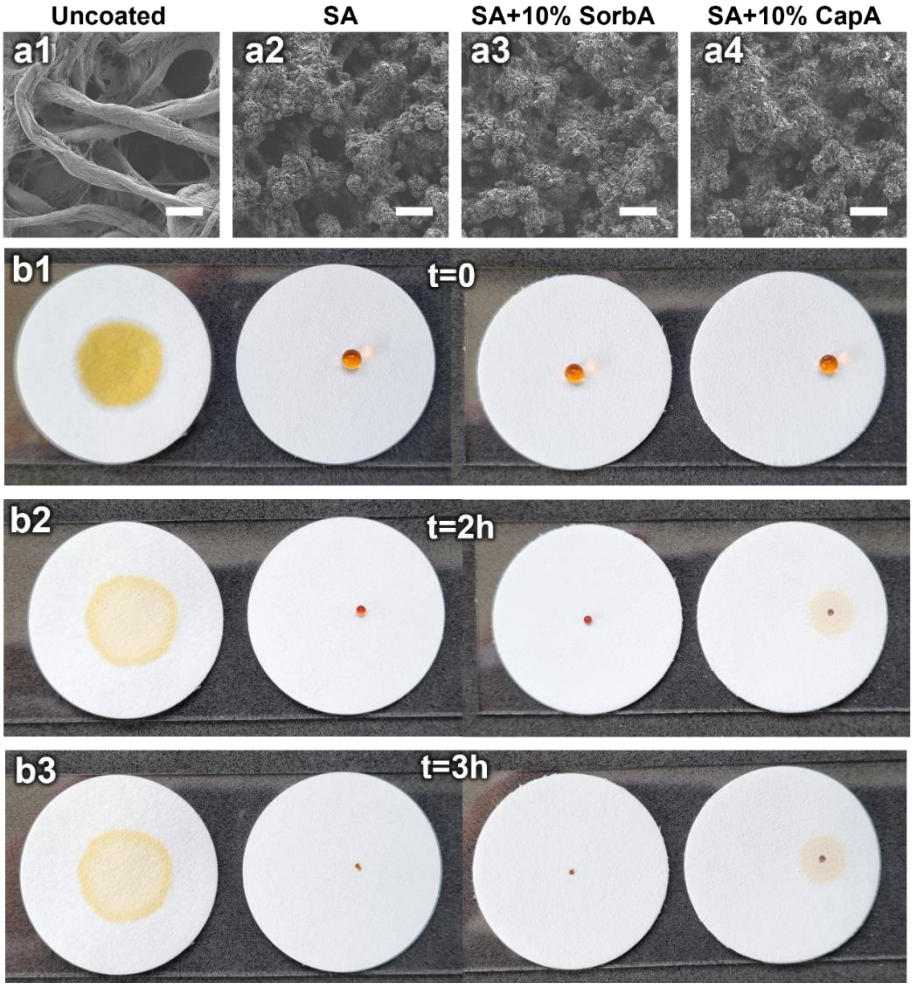


*SI 7: (a1-a4) HR-SEM images of uncoated paper and different coatings deposited on paper. (a1) Uncoated paper. (a2) Stearic acid coating. (a3) Stearic with 10% sorbic acids coating. (a4) Stearic with 10% caprylic acids coating. Scalebar is 30 µm. (b1-b3) Methyl orange-stained water droplet on dry samples over time. (b1) At t=0. (b2) After 2 hours. (b3) After 3 hours. Samples from left to right: uncoated paper, stearic acid coated paper, stearic with 10% sorbic acid coated paper, stearic with 10% caprylic acids coated paper.*

The water droplet is not absorbed and remains stable over 2 hours on pure stearic acid coating and stearic with 10% sorbic acids coating (SI 7 b1, b2). In the case of stearic with 10% caprylic acid coating, partial water absorption into the paper through the coating takes place, but after 2 hours, an unabsorbed droplet still exists (SI 7 b1, b2). Despite the cover, the droplets completely evaporated after 3 hours, and the remaining methyl orange spots indicate the low contact area between the droplet and the coating. That result proves the stable superhydrophobicity of stearic acid coating and stearic acid with 10% sorbic acid coating over time (SI 7 b3).

XRD of the coatings after immersion in water:

XRD of different coatings after immersion in water are shown in SI 8:

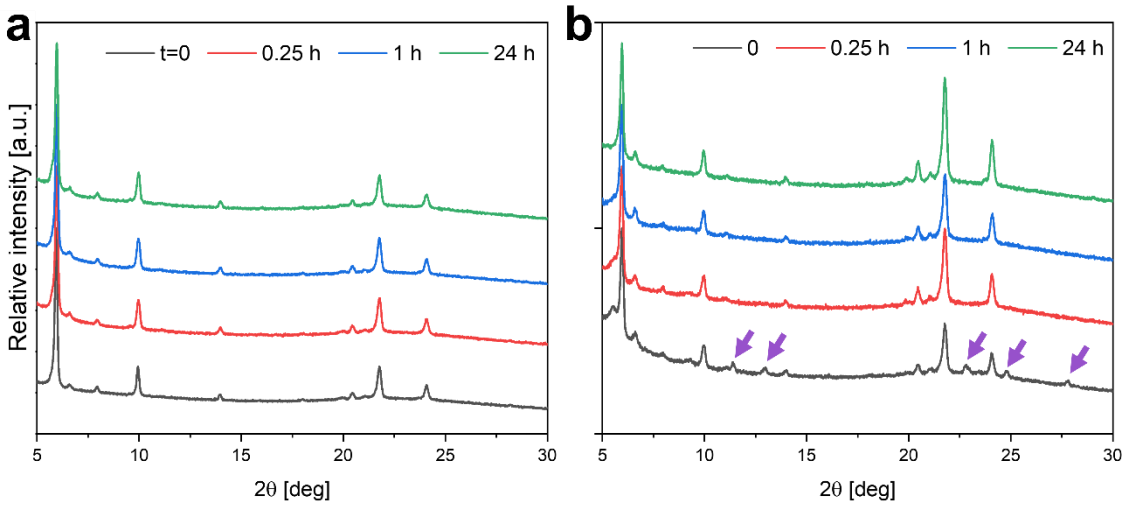


*SI 8: XRD of coatings after immersion in water for 15 min, 1 h and 24 h. (a) Stearic with 20% caprylic acid coating. (b) Stearic with 20% sorbic acid coating.*

Despite the evolution of the morphology upon immersion of the coating with caprylic acid in water (Figure 4 a-c) and the evidence of caprylic acid release from the coating (Figure 4 e), no significant change was found in the structure (SI 8 a). In the case of sorbic acid addition, the peaks related to the sorbic acid disappear after immersion in water for 15 min (SI 8 b, purple arrows). The increasing absorbance peak of the analyzed water (Figure 4) indicates the continuation of the release of sorbic acid from the coating from deeper zones that are probably not reached by X-ray in the measurement setup.

Evaluation of caprylic acid release at ambient conditions:

To prove our assumption that caprylic acid is released to the atmosphere during storage at ambient conditions, an accelerated conditions study was performed using TGA analysis. Freshly prepared samples of pure stearic acid, or stearic with 20% caprylic acid were mechanically detached from the glass substrate and the weight loss at 45°C with constant air flow was measured. SI 9 a show the weight loss as a result of caprylic acid release over time, with calculated weight decrease of 10.4% over 10 hours. No weight loss was detected for the pure stearic acid sample (SI 9 c). Subsequently, high-resolution TGA was implemented for determination of the remaining caprylic acid in the sample after 10 hours at 45°C. The results shown in SI 9 b indicate a corresponding weight loss of 10.7% related to evaporation of caprylic acid before the main weight loss related to stearic acid evaporation occurs (see SI 9 d for pure stearic acid sample).

To assure the release of caprylic acid to the atmosphere during storage at ambient conditions in non-accelerated study, identical samples (round, 18 mm in diameter glass slides, coated with stearic + 20% caprylic acid) were immersed in 5 ml of double-distilled water for 1 h after different storage periods: freshly prepared (t=0), after 3 days, and after 11 days of storage. After 1 hour of immersion, 200 µL aliquots of the aqueous medium were collected and absorbance measurements were carried out. The results show a decrease in the absorbance intensity of the peak at 265 nm (characteristic of caprylic acid), for samples that stored for a longer period prior to immersion in water, indicating a lower concentration of caprylic acid after longer storage (SI 9 e). This experiment suggests that a lower content of caprylic acid remains in the in the coating after storage at ambient conditions.

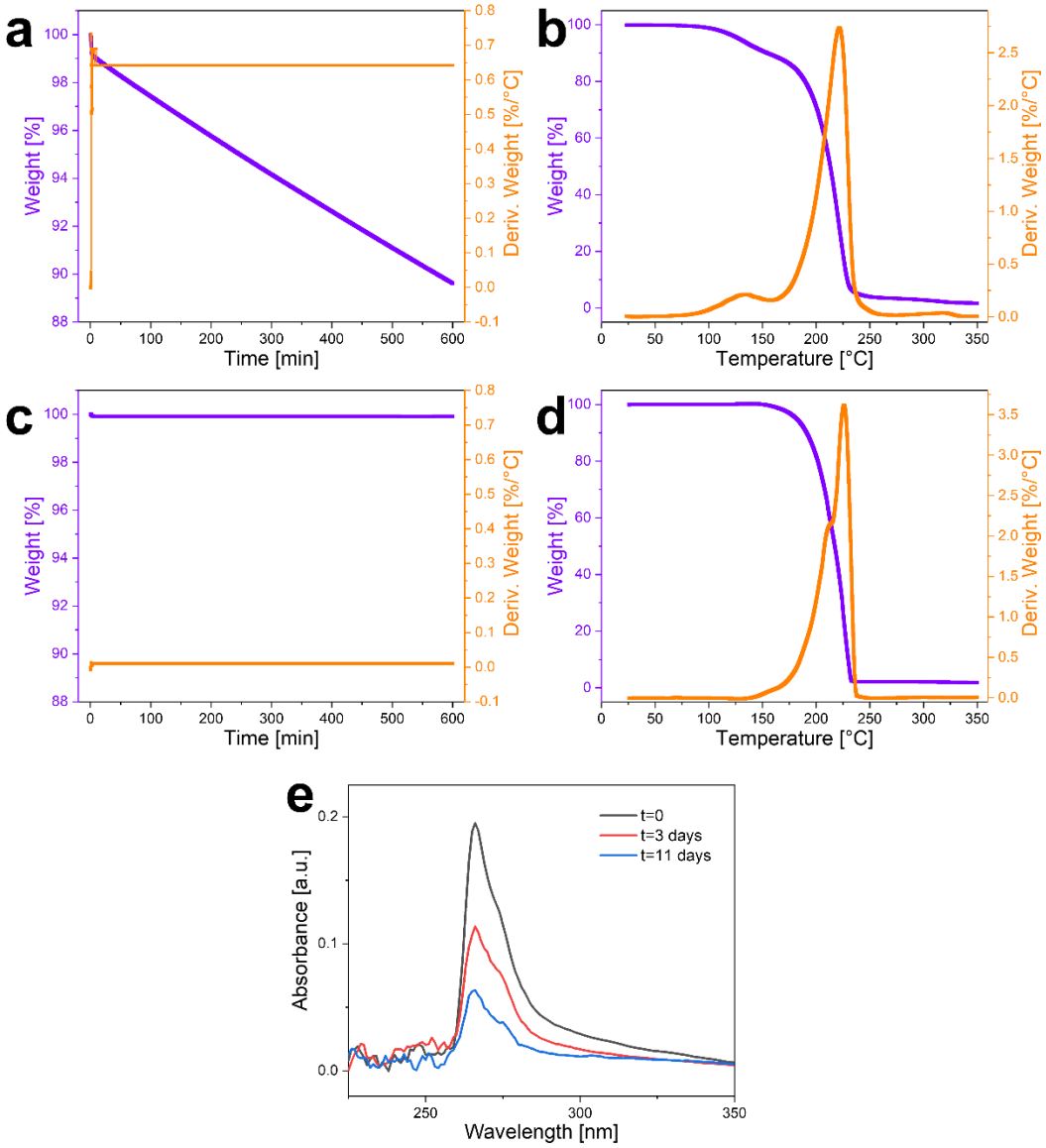


*SI 9: Thermogravimetric analysis of coatings: (a,c) Thermograms and corresponding (first derivative) dTGA curves of detached stearic acid with 20% caprylic acid and stearic acid coatings, respectively, under isothermal conditions of 45°C for 10 hours under air atmosphere. (b,d) Dynamic high-resolution TGA and dTGA results for the stearic acid with 20% caprylic acid and stearic acid coatings, respectively, subsequently performed after the isothermal step (10 hours at 45°C). (e) Corresponding absorbance spectra of the collected aqueous media following 1-hour immersion of the stearic acid with 20% caprylic acid coating, stored for different periods at ambient conditions.*

Investigation of intrinsic antifungal properties of the studied fatty acids:

To elucidate the mode of action of our coatings against *B. cinerea*, we have characterized the intrinsic antifungal activity of the selected fatty acids in their native form (as powder or a liquid) by the agar diffusion method. To this end, 50 mg of each fatty acid was placed in the center of a petri dish containing *B. cinerea*-infected agar. The samples were incubated for 7 days at 24°C, and mycelium growth was examined.

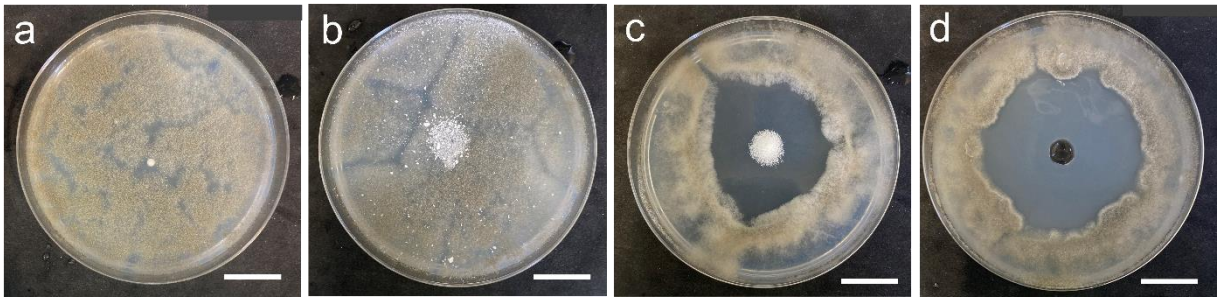


*SI 10: Digital images of B. cinerea growth on PDA agar (t=7 days) with: (a) Control (without added fatty acid). (b) Stearic acid. (c) Sorbic acid. (d) Caprylic acid. Scalebar is 2 cm.*

The results shown in SI 10 reveal that pure stearic acid powder exhibits no inhibition effect on *B. cinerea* growth compared to the control agar sample without fatty acids (SI 10 b vs. a). In contrast, both pure sorbic and caprylic acids inhibit *B. cinerea* growth, with inhibition rates of 52 ± 10% and 64 ± 8%, respectively. The enhanced inhibition effect of MCFAs in this experiment may be attributed to their higher diffusion rate in agar compared to the long-chain stearic acid molecule. While this method cannot definitively exclude stearic acid's inhibition of *B. cinerea* growth, it clearly highlights the superior intrinsic antimicrobial effects of caprylic and sorbic acids relative to stearic acid in their native forms.